ESCUELA TÉCNICA SUPERIOR DE INGENIERÍA EN SISTEMAS DE TELECOMUNICACIÓN

UNIVERSIDAD POLITÉCNICA DE CARTAGENA

Departamento de Tecnologías de la Información y la Comunicación

TRABAJO FIN DE GRADO

Diseño de nuevos filtros en guía rectangular basados en aperturas resonantes

Grado en Ingeniería en Sistemas de Telecomunicación

Universidad Politécnica de Cartagena

Escuela Técnica Superior Ingeniería de Telecomunicación

Autora: Eva Bernal Nicolás
Director: Alejandro Álvarez Melcón
Codirectora: Celia Gómez Molina

Index

1. Introduction **6**
1.1. State of the art and application 6

2. Technology characterization **8**
2.1. Introduction 8
2.2. Resonant frequency 9
2.3. External quality factor (Q_{ext}) 12
2.4. Unloaded quality factor (Q_u) 16
2.5. Inter-resonator coupling (k) 19
2.5.1. Comparative between inter-resonator coupling (k) for the different sizes of apertures. . 33
2.6. Transmission zeros (TZ) 34

3. Filter design with FEST3D **38**
3.1. Introduction 38
3.2. Design of a 500 MHz bandwidth filter in Ku-band 39
3.3. Design of a 1 GHz bandwidth filter in Ku-band 48
3.4. Design of a 2 GHz bandwidth filter in Ku-band 55
3.5. Advantages of the proposed technology 62

4. Conclusions and further work **65**
4.1. Conclusions 65
4.2. Further work 65

List of Figures

1.1. Filters in a typical satellite communication subsystem block diagram (reproduced from [3]). . 6

2.1. Structure under analysis. It is composed by two thick apertures of size $ap \times bp \times l_{th}$ coupled by a WR-75 waveguide section of dimensions 19.05 mm × 9.525 mm and length l. 8
2.2. Equivalent circuit for the resonant aperture. 9
2.3. Aperture acting as a resonator and its dimensions. 10
2.4. Structure under analysis. It is composed by two WR-75 waveguide sections connected by a thick resonant aperture of size $ap \times bp \times l_{th}$. 10
2.5. Variation of the resonant frequency (f_0) as a function of the aperture's width (ap). 11
2.6. Variation of the resonant frequency (f_0) as a function of the aperture's height (bp). 11
2.7. Resonant frequency (f_0) for different aperture's thickness (l_{th}). 12
2.8. Variation of the Δ_{3dB} as a function of ap, for different values of l_{th}. 14
2.9. Variation of the Q_{ext} as a function of ap, for different values of l_{th}. 15
2.10. Structure under analysis for the Q_u calculation, with Alumimun background (σ = 38000000 S/m) and without input/output ports. 16
2.11. Variation of the Q_u as a function of ap for different l_{th}. 18
2.12. Structure simulated to obtain the inter-resonator coupling, applying a symmetry plane (pink surface) to a structure composed of two symmetric coupled resonators. 19
2.13. Inter-resonator coupling as a function of l (mm) for different l_{th} (mm) for a 13 mm × 0.2 mm iris. 22
2.14. Inter-resonator coupling as a function of l (mm) for different l_{th} (mm) for a 13.05 mm × 0.45 mm iris. 24
2.15. Inter-resonator coupling as a function of l (mm) for different l_{th} (mm) for a 13.1 mm × 0.7 mm iris. 26
2.16. Inter-resonator coupling as a function of l (mm) for different l_{th} (mm) for a 13.3 mm × 1.7 mm iris. 28
2.17. Inter-resonator coupling as a function of l (mm) for different l_{th} (mm) for a 13.5 mm × 2.6 mm iris. 30
2.18. Inter-resonator coupling as a function of l (mm) for different l_{th} (mm) for a 14 mm × 3.8 mm iris. 32
2.19. Inter-resonator coupling for the resonant aperture's dimensions under study. 33
2.20. Structure under analysis with step discontinuities to implement transmission zeros. 34
2.21. S parameters response for the filter in Fig. 2.21 for two different l_{disc} values. 35
2.22. S parameters response of the filter in Fig. 2.21 for different widths and heights of the step while keeping constant l_{disc} = 1.5 mm. 36
2.23. Asymmetric structure for the independent control of the two transmission zeros. 36
2.24. Resonant frequency of transmission zeros for the asymmetric filter in Fig. 2.23. 37

3.1. Generic structure of the third order filter under analysis. 39
3.2. Variation of the Q_{ext} as a function of ap, for different l_{th}. 40

3.3. Inter-resonator coupling as a function of l (mm), for different l_{th} (mm), for a 13.05 mm × 0.45 mm resonant iris. . . . 41
3.4. S parameters response of the initial point for the 500 MHz bandwidth filter. . . . 42
3.5. S parameters response of the optimized 500 MHz bandwidth filter. . . . 43
3.6. Optimized geometry for the 500 MHz bandwidth filter. . . . 44
3.7. Optimized geometry for the 500 MHz bandwidth filter with two step discontinuities. . . . 45
3.8. S parameters response of the 500 MHz bandwidth filter when adding two 25.05 mm × 15.525 mm × 2 mm step discontinuities. . . . 46
3.9. S parameters response of the 500 MHz bandwidth filter when adding two 26.05 mm × 16.525 mm × 2 mm step discontinuities. . . . 47
3.10. Variation of the Q_{ext} as a function of *ap*, for different l_{th}. . . . 48
3.11. Inter-resonator coupling as a function of l (mm), for different l_{th} (mm), for a 13 mm × 0.2 mm iris. . . . 49
3.12. S parameters response of the first aproximation for the 1 GHz bandwidth filter. . . . 50
3.13. S parameters response of the first optimization for the 1 GHz bandwidth filter. . . . 51
3.14. First optimized geometry for the 1 GHz bandwidth filter. . . . 52
3.15. S parameters response of the second optimization for the 1 GHz bandwidth filter. . . . 52
3.16. Final optimized geometry of the 1 GHz bandwidth filter. . . . 53
3.17. S parameter comparison of the two optimizations for the 1 GHz bandwidth filter. . . . 54
3.18. Variation of the Q_{ext} as a function of *ap*, for different l_{th}. . . . 55
3.19. Inter-resonator coupling as a function of l (mm), for different l_{th} (mm), for a 13.5 mm × 2.6 mm iris. . . . 56
3.20. S parameters reponse of the first aproximation for the 2 GHz bandwidth filter. . . . 57
3.21. S parameters reponse of the optimized design for the 2 GHz bandwidth filter. . . . 58
3.22. Optimized geometry for the 2 GHz bandwidth filter. . . . 59
3.23. Optimized geometry for the 2 GHz bandwidth filter with two step discontinuities. . . . 60
3.24. S parameters response of the 2 GHz bandwidth filter when adding a 25.05 mm × 15.525 mm × 2 mm step discontinuity. . . . 60
3.25. S parameters response of the 2 Ghz bandwidth filter when adding two differenciated transmission zeros. . . . 61
3.26. Out of band response of the 500 MHz filter using resonant apertures. . . . 62
3.27. Out of band response of the 500 MHz filter using resonant cavities. . . . 63
3.28. Optimized geometry of the filter based in resonant cavities. . . . 64

List of Tables

2.1. Δ_{3dB} and Q_{ext} for different dimensions of the aperture when $l_{th} = 0.01$ mm. 13
2.2. Δ_{3dB} and Q_{ext} for different dimensions of the aperture when $l_{th} = 1$ mm. 13
2.3. Δ_{3dB} and Q_{ext} for different dimensions of the aperture when $l_{th} = 2$ mm. 13
2.4. Δ_{3dB} and Q_{ext} for different dimensions of the aperture when $l_{th} = 3$ mm. 14
2.5. Δ_{3dB} and Q_{ext} for different dimensions of the aperture when $l_{th} = 5$ mm. 14
2.6. Q_u for different dimensions of the aperture when $l_{th} = 0.01$ mm. 17
2.7. Q_u for different dimensions of the aperture when $l_{th} = 1$ mm. 17
2.8. Q_u for different dimensions of the aperture when $l_{th} = 2$ mm. 17
2.9. Q_u for different dimensions of the aperture when $l_{th} = 3$ mm. 17
2.10. Q_u for different dimensions of the aperture when $l_{th} = 5$ mm. 18
2.11. Order of magnitude of the typical Q_u values for different technologies. 19
2.12. Inter-resonator coupling as a function of l (mm) for a 13 mm × 0.2 mm × 0.01 mm iris. . . . 20
2.13. Inter-resonator coupling as a function of l (mm) for a 13 mm × 0.2 mm × 1 mm iris. 20
2.14. Inter-resonator coupling as a function of l (mm) for a 13 mm × 0.2 mm × 2 mm iris. 21
2.15. Inter-resonator coupling as a function of l (mm) for a 13 mm × 0.2 mm × 3 mm iris. 21
2.16. Inter-resonator coupling as a function of l (mm) for a 13 mm × 0.2 mm × 5 mm iris. 21
2.17. Inter-resonator coupling as a function of l (mm) for a 13.05 mm × 0.45 mm × 0.01 mm iris. . 22
2.18. Inter-resonator coupling as a function of l (mm) for a 13.05 mm × 0.45 mm × 1 mm iris. . . 22
2.19. Inter-resonator coupling as a function of l (mm) for a 13.05 mm × 0.45 mm × 2 mm iris. . . 23
2.20. Inter-resonator coupling as a function of l (mm) for a 13.05 mm × 0.45 mm × 3 mm iris. . . 23
2.21. Inter-resonator coupling as a function of l (mm) for a 13.05 mm × 0.45 mm × 5 mm iris. . . 23
2.22. Inter-resonator coupling as a function of l (mm) for a 13.1 mm × 0.7 mm × 0.01 mm iris. . . 24
2.23. Inter-resonator coupling as a function of l (mm) for a 13.1 mm × 0.7 mm × 1 mm iris. 24
2.24. Inter-resonator coupling as a function of l (mm) for a 13.1 mm × 0.7 mm × 2 mm iris. 25
2.25. Inter-resonator coupling as a function of l (mm) for a 13.1 mm × 0.7 mm × 3 mm iris. 25
2.26. Inter-resonator coupling as a function of l (mm) for a 13.1 mm × 0.7 mm × 5 mm iris. 25
2.27. Inter-resonator coupling as a function of l (mm) for a 13.3 mm × 1.7 mm × 0.01 mm iris. . . 26
2.28. Inter-resonator coupling as a function of l (mm) for a 13.3 mm × 1.7 mm × 1 mm iris. 26
2.29. Inter-resonator coupling as a function of l (mm) for a 13.3 mm × 1.7 mm × 2 mm iris. 27
2.30. Inter-resonator coupling as a function of l (mm) for a 13.3 mm × 1.7 mm × 3 mm iris. 27
2.31. Inter-resonator coupling as a function of l (mm) for a 13.3 mm × 1.7 mm × 5 mm iris. 27
2.32. Inter-resonator coupling as a function of l (mm) for a 13.5 mm × 2.6 mm × 0.01 mm iris. . . 28
2.33. Inter-resonator coupling as a function of l (mm) for a 13.5 mm × 2.6 mm × 1 mm iris. 28
2.34. Inter-resonator coupling as a function of l (mm) for a 13.5 mm × 2.6 mm × 2 mm iris. 29
2.35. Inter-resonator coupling as a function of l (mm) for a 13.5 mm × 2.6 mm × 3 mm iris. 29
2.36. Inter-resonator coupling as a function of l (mm) for a 13.5 mm × 2.6 mm × 5 mm iris. 29
2.37. Inter-resonator coupling as a function of l (mm) for a 14 mm × 3.8 mm × 0.01 mm iris. . . . 30
2.38. Inter-resonator coupling as a function of l (mm) for a 14 mm × 3.8 mm × 1 mm iris. 30
2.39. Inter-resonator coupling as a function of l (mm) for a 14 mm × 3.8 mm × 2 mm iris. 31
2.40. Inter-resonator coupling as a function of l (mm) for a 14 mm × 3.8 mm × 3 mm iris. 31

2.41. Inter-resonator coupling as a function of l (mm) for a 14 mm × 3.8 mm × 5 mm iris. 31

3.1. Requirements for the filters to be designed in this chapter. 38
3.2. Initial dimensions for the 500 MHz bandwidth filter, according to the schematic shown in Fig. 3.1. 41
3.3. Final dimensions for the 500 MHz bandwidth filter. 43
3.4. Comparative between the initial and final dimensions for the 500 MHz bandwidth filter. . . . 44
3.5. Final dimensions for the 500 MHz bandwidth filter when adding two 25.05 mm × 15.525 mm × 2 mm step discontinuities. 46
3.6. Final dimensions for the 500 MHz bandwidth filter when adding two 26.05 mm × 16.525 mm × 2 mm step discontinuities. 47
3.7. Initial dimensions for the 1 GHz bandwidth filter. 49
3.8. Final dimensions of the first optimization for the 1 GHz bandwidth filter. 51
3.9. Final dimensions of the second optimization for the 1 GHz bandwidth filter. 53
3.10. Comparative between the dimensions of the 1 GHz bandwidth filter for the two optimizations. 54
3.11. Final size comparison between the two optimizations for the 1 GHz bandwidth filter. 55
3.12. Initial dimensions for the 2 GHz bandwidth filter. 56
3.13. Final dimensions for the 2 GHz bandwidth filter. 58
3.14. Comparative between the initial and final dimensions for the 2 GHz bandwidth filter. 59
3.15. Final dimensions for the 1 GHz bandwidth filter when adding a 25.05 mm × 15.525 mm × 2 mm step discontinuity. 61
3.16. Comparative between the two filters under study. 64

Chapter 1

Introduction

1.1. State of the art and application

The history of satellites dates back to 1957, when the Sputnik I was launched by the Soviet Union. Over the years, satellites have been modernized and their performance has improved considerably [1].
The two most common satellite orbits are geostationary (GEO) and polar orbiting. A geostationary satellite travels from west to east over the equator. It moves in the same direction and at the same speed as the Earth, so they observe a particular area continuously. However, they cannot observe the polar regions due to the Earth's curvature, which is a limitation. Polar orbiting satellites travel from pole to pole in a north south direction. They usually fly at low altitudes, have less resolution than geostationary satellites and do not move at the same rate Earth is spinning. Because of this, they do not observe a specific area of the Earth, but the whole planet. Therefore, it is the combination of these two types of satellites what provides the capability of continuous observation of the Earth, as they complement each other [2].
One example of satellites are repeaters, that receive radio signals transmitted from the Earth, amplify them, translate them in frequency, and retransmit them back to the ground. The typical block diagram of a communication subsystem of a satellite repeater, as explained in [3], is shown in Fig. 1.1.

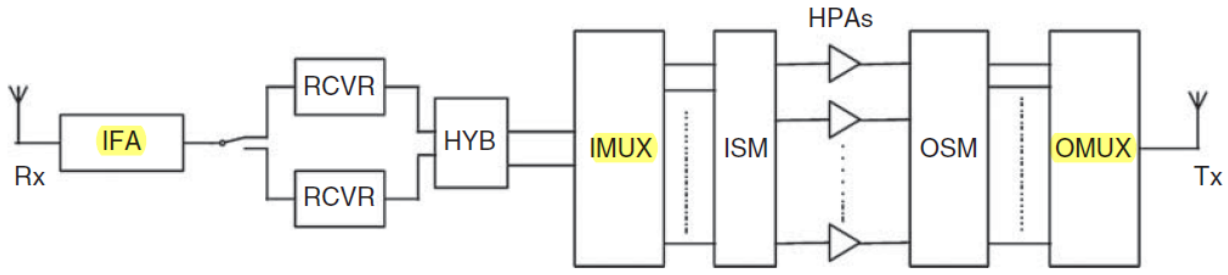

Figure 1.1: Filters in a typical satellite communication subsystem block diagram (reproduced from [3]).

As we can see, among the components found in satellites we can find several filters. Filters are electronic devices that are used to allow certain frequencies, rejecting the rest of the frequency bands. The range of frequencies that the filter allows is called *pass band*, while the range of frequencies rejected by the filter is called *rejected band*.
Filters must meet a number of specifications, such as low loss, high power handling, and they also must work in a certain frequency with a determined bandwith. These specifications usually depend on the application. Furthermore, as seen in Fig. 1.1, filters are often part of IMUX (Input Multiplexing Filter Network) or OMUX (Output Multiplexing Network). These channelizing filter networks normally have a strong requirement on the isolation level in the adjacent band. To meet these restricted out of band requirements, it

is often needed the use of filters with transmission zeros just outside the passband, in order to fulfill this isolation response. In adition to all these electrical requirements, there are also physical constraints such as size, mass and manufacturing cost [3].

There are several applications for satellites, such as communications, navigation or downstream. In this work we are going to focus on an application that is becoming more and more relevant these days: the environmental application.
The main goal of Earth observation satellites is to monitor the conditions of the Earth's environment, such as stratospheric ozone depletion, agriculture, pollution, sea ice monitoring or sea level monitoring, contributing in this way to the study of climate change and oceanography [1].
Depending on the specific application, the satellite's filters will work in a specific band, based on the size of the particles or objects we want to detect.
For this project, we have chosen the detection of floating plastics in the ocean. Plastic debris, such as water bottles, fishing nets and grocery bags are a real danger for the environment, and therefore, the monitorization of areas with high concentration of floating plastics can help optimizing the ocean clean up, by creating a hot spot map of the world with the highest plastic debris concentration.
Given the high power and high performance requirements needed for this application, waveguide technology was chosen for this project [4]. However, the disadvantages of this technology for space applications are its weight and volume. This is why there is currently a lot of research around new lighter and more compact filters [5]. In order to detect plastic debris in the ocean, we will work in Ku-band with the WR-75 standard. For this, a novel technology based on resonant apertures located along a WR-75 waveguide is proposed. In this new technology, the resonance is produced due to the discontinuity between the WR-75 waveguide section and the aperture.
This bachelor thesis is organized as follows. We will begin in Chapter 2 by explaining the proposed technology through its characterization. We will obtain the external quality factor (Q_{ext}), the unloaded quality factor (Q_u) and the inter-resonator coupling (k). We will then explain how to incorporate transmission zeros to meet the out of band requirements. In Chapter 3 we will discuss various designs using this technology, and we will outline the advantages of this technology. The conclusions and further work are explained in Chapter 4.

Chapter 2

Technology characterization

2.1. Introduction

In this chapter we will characterize the proposed technology for the realization of compact Ku-band filters. For this, we will use the WR-75 standard for rectangular waveguides, which dimensions (Port1_a × Port1_b) are 19.05 mm × 9.525 mm. These filters are based on resonant apertures coupled by propagating WR-75 waveguide sections, as shown in Fig. 2.1.
Throughout this chapter we will study how to adjust the aperture's resonant frequency (f_0) and how to obtain a determined external quality factor (Q_{ext}) based on the input/output coupling requirements. Besides, we will study the unloaded quality factor (Q_u) of the proposed resonators and how to adjust the inter-resonator coupling (k). We will also study how to implement topologies with transmission zeros (TZ) using the proposed technology.

The structure under study is composed of resonant apertures located along a WR-75 waveguide section. This structure is shown in Fig. 2.1, where we have included the names of the variables to facilitate the comprehension of the text.

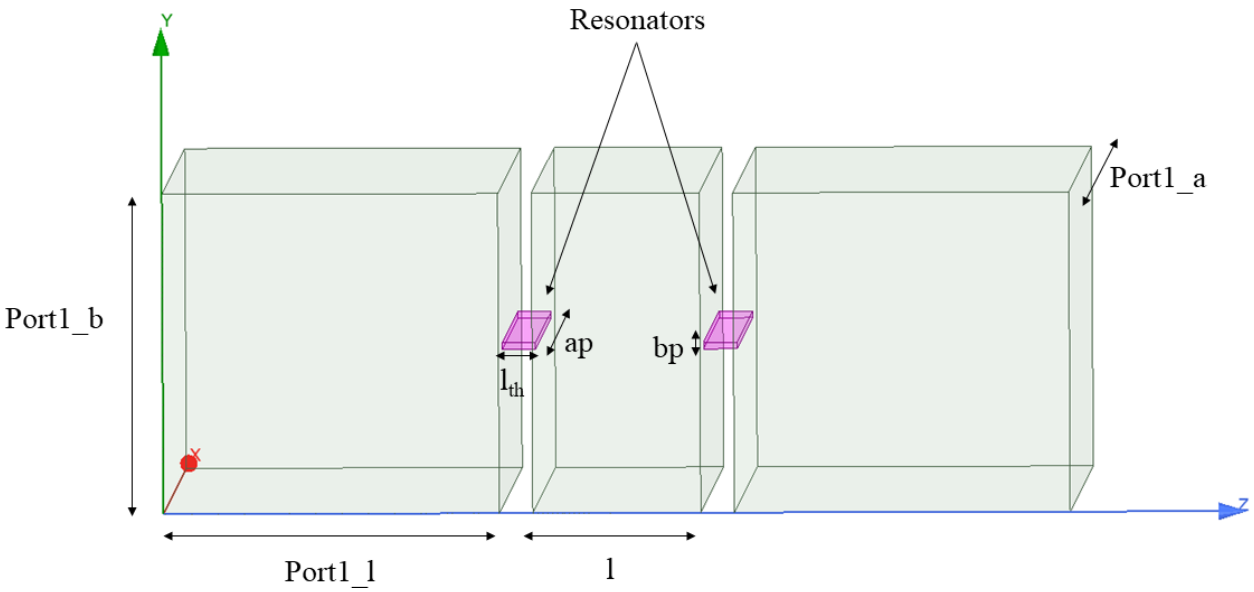

Figure 2.1: Structure under analysis. It is composed by two thick apertures of size $ap \times bp \times l_{th}$ coupled by a WR-75 waveguide section of dimensions 19.05 mm × 9.525 mm and length l.

In this structure, the size of the aperture ($ap \times bp$) controls the resonant frequency (f_0). The thickness of the aperture (l_{th}) can be used to adjust the external quality factor (Q_{ext}). Finally, it will be possible to control the inter-resonator coupling (k) with the length of the intermediate waveguide section (l).
In order to characterize the technology, we will do the following tests:

- A Frequency Domain analysis to study how to control the resonant frequency (f_0) and to obtain the external quality factor (Q_{ext}).
- An Eigenmode Solver analysis to obtain the unloaded quality factor (Q_u) and the inter-resonator coupling (k).

2.2. Resonant frequency

In the filtering structure proposed in Fig. 2.1, the resonance, instead of being produced by a traditional $\lambda/2$ cavity, is produced by the discontinuity between the WR-75 waveguide section and the aperture (see Fig. 2.1). This resonance can be modeled as the parallel of a capacitor and an inductance, as follows:

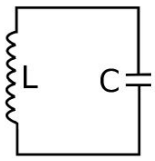

Figure 2.2: Equivalent circuit for the resonant aperture.

Therefore, the resonant angular frequency (ω_0) can be calculated as:

$$\omega_0 = \frac{1}{\sqrt{LC}}, \tag{2.1}$$

where L and C are the equivalent inductance and capacitor (see Fig. 2.2).
In the proposed technology, the resonant frequency can be controlled through the variation of the aperture's dimensions, which are shown in Fig. 2.3. To see how to control the resonant frequency of the aperture, we perform a first test in ANSYS HFSS [6] using the structure shown in Fig. 2.4. As we can see in Fig. 2.4, we simulate a single aperture of dimensions $ap \times bp \times l_{th}$. In this test, we fix the length of the aperture (l_{th}) to 1 mm and we vary the width (ap) and the height (bp) of the aperture to see how these parameters modify the resonant frequency. The results of these tests are reported in Fig. 2.5 and Fig. 2.6.

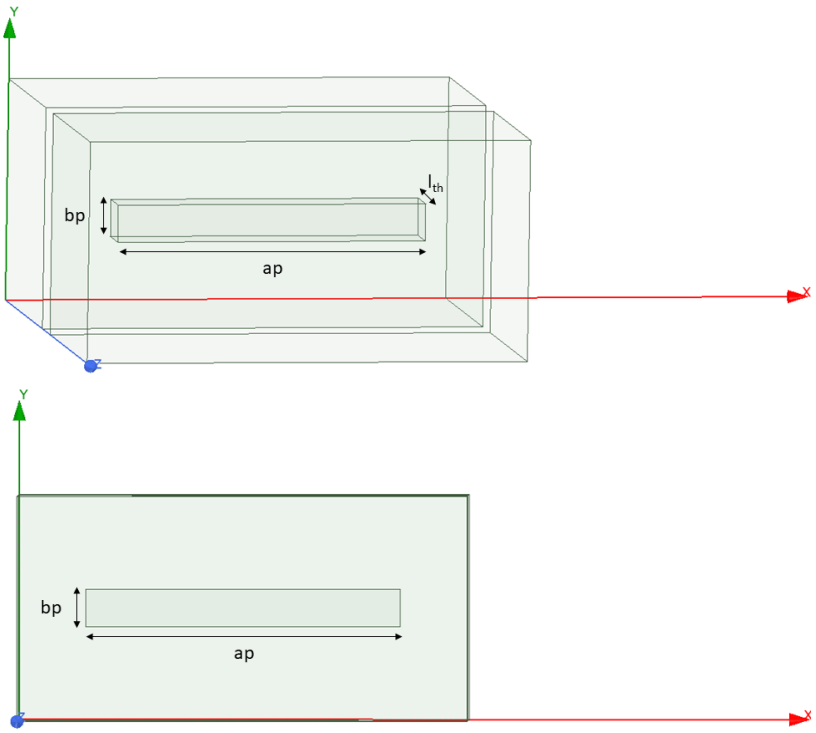

Figure 2.3: Aperture acting as a resonator and its dimensions.

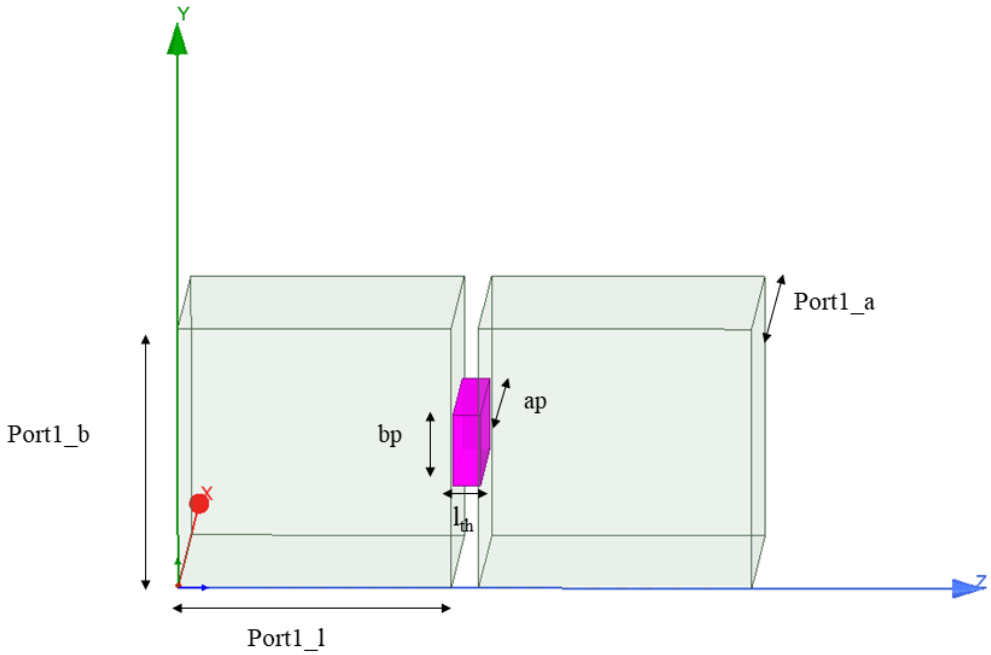

Figure 2.4: Structure under analysis. It is composed by two WR-75 waveguide sections connected by a thick resonant aperture of size $ap \times bp \times l_{th}$.

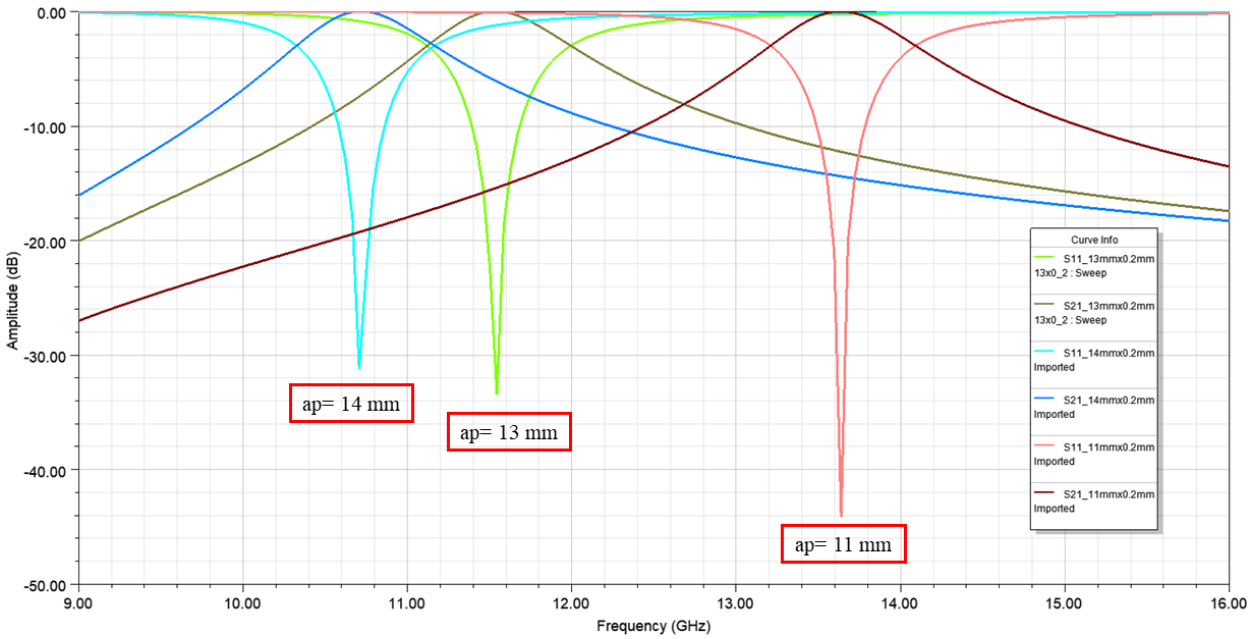

Figure 2.5: Variation of the resonant frequency (f_0) as a function of the aperture's width (ap).

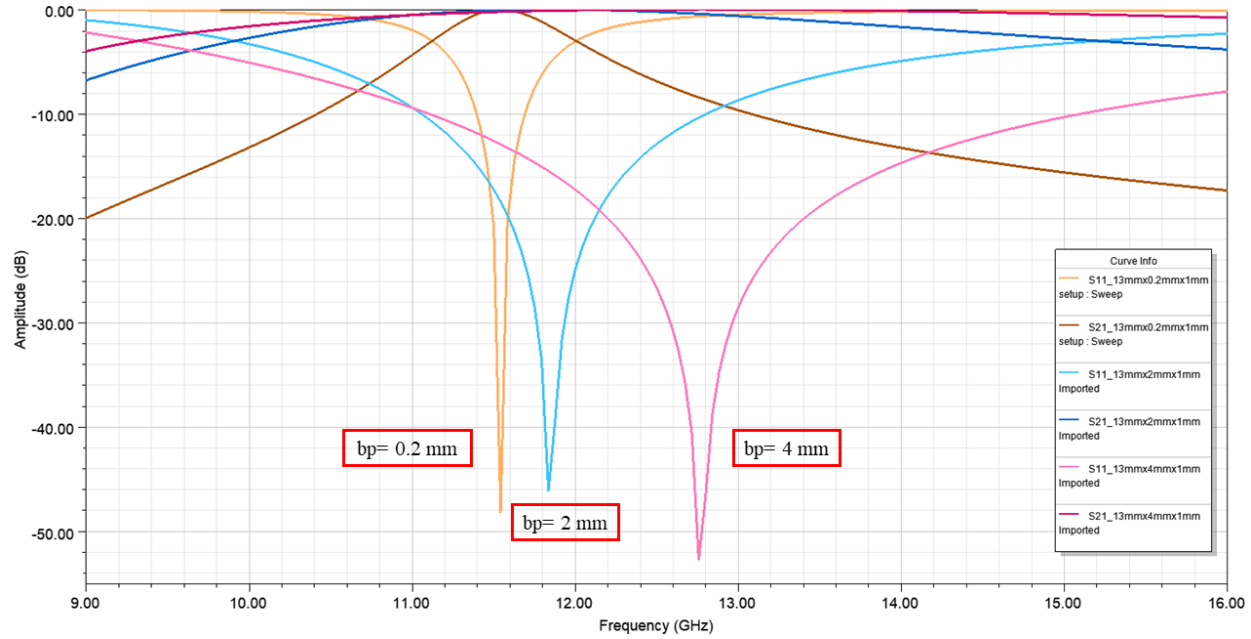

Figure 2.6: Variation of the resonant frequency (f_0) as a function of the aperture's height (bp).

As observed in Fig. 2.5, if the width of the iris (ap) is increased, a decrement in the resonant frequency is observed. Therefore, the resonant frequency (f_0) is inversely proportional to ap. However, as we can see in Fig. 2.6, when increasing the height of the aperture (bp), the resonant frequency increases.
In order to study the variation of the resonant frequency (f_0) as a function of the aperture's thickness (l_{th}), we have performed a second test where we keep fixed the aperture's width and height ($ap \times bp$) to 13 mm $\times$ 0.2 mm, and we vary the aperture's thickness. The results are reported in Fig. 2.7.

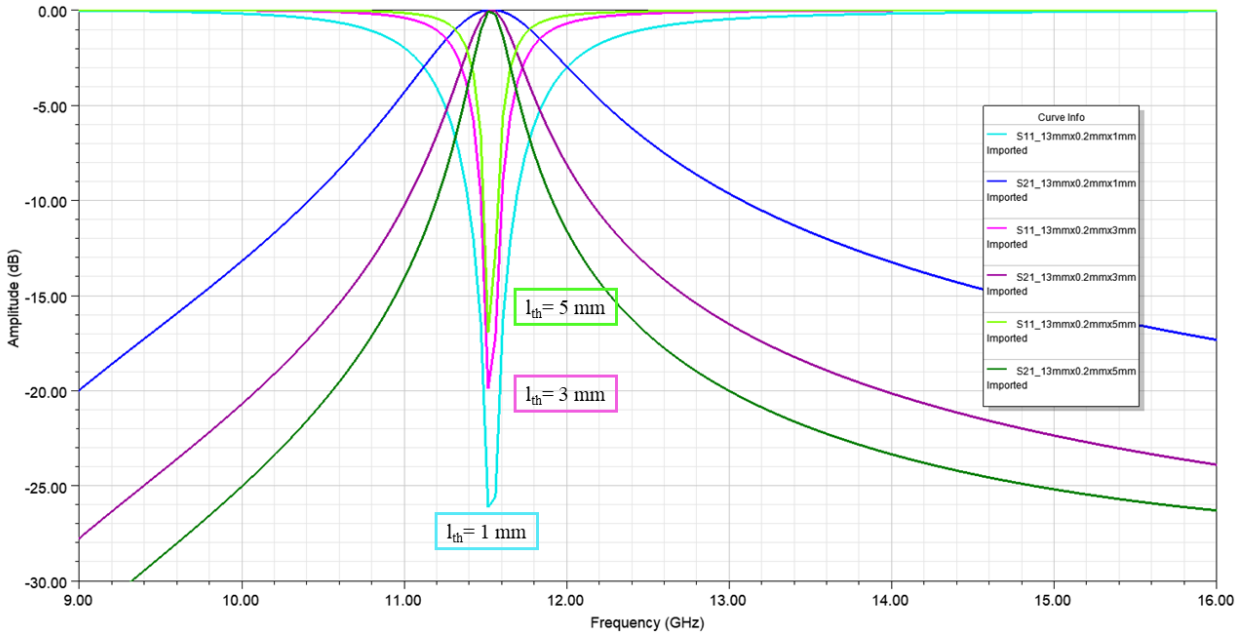

Figure 2.7: Resonant frequency (f_0) for different aperture's thickness (l_{th}).

As we can see in Fig. 2.7, the resonant frequency (f_0) does not depend on the thickness of the aperture (l_{th}).
For this project, in order to fix the center frequency of the filter to 11.5 GHz, we have chosen the following sizes of apertures ($ap \times bp$): 13 mm $\times$ 0.2 mm, 13.3 mm $\times$ 1.7 mm, 13.5 mm $\times$ 2.6 mm and 14 mm $\times$ 3.8 mm. Besides, we observed a sensitive behaviour of the structure around ap= 13 mm, and that is why we added two more sizes of apertures ($ap \times bp$): 13.05 mm $\times$ 0.45 mm and 13.1 mm $\times$ 0.7 mm, that also mantain the center frequency in 11.5 GHz. It should be noted that we have set a minimum value for the height of the aperture (bp) of 0.2 mm, so that the filter can be manufactured.

2.3. External quality factor (Q_{ext})

"The external quality factor (Q_{ext}) is defined as the ratio of the stored energy in a resonator to the power loss in the input/output feed source", as explained in [7]:

$$Q_{ext} = \omega_0 \frac{W_T}{P_{ext}}, \tag{2.2}$$

where w_0 is the radian resonant frequency, W_T is the average energy stored, and P_{ext} is the power dissipated in the input/output source.
It is used to measure the coupling between the first resonator and the source, as well as the coupling between the last resonator and the load, that is, the input/output couplings. It also can be calculated as two times

the quotient of the resonant frequency (f_0) and the 3dB bandwidth (Δ_{3dB}):

$$Q_{ext} = 2\ \frac{f_o}{\Delta_{3dB}} \tag{2.3}$$

Therefore, it is inversely proportional to the 3 dB bandwith (Δ_{3dB}), which means that to obtain a high Q_{ext}, the 3 dB bandwidth (Δ_{3dB}) must be small, and this leads to a low external coupling.
In the proposed structure, the Q_{ext} can also be controlled by changing the dimensions of the iris. The structure simulated in order to do this test can be seen in Fig. 2.4. This structure consists in a resonant aperture excited by two WR-75 waveguide sections.
To characterize this parameter, different values for the aperture's width (ap) have been chosen, and then the height (bp) has been adjusted in order to mantain the resonant frequency (f_0) fixed, as explained in the introduction. Besides, we have performed tests for different aperture's thickness (l_{th}), observing how this variable affects the external quality factor, and therefore, the input/output coupling. All the values used for the different variables as well as the measured 3 dB bandwidth (Δ_{3dB}) and Q_{ext} are presented in Tables 2.1 - 2.5.

ap (mm)	bp (mm)	f_0 (GHz)	Δ_{3dB} (GHz)	Q_{ext}
13	0.2	11.41	2.74	8.33
13.05	0.45	11.41	3.62	6.30
13.1	0.7	11.4	4.39	5.20
13.3	1.7	11.41	7.36	3.10
13.5	2.6	11.42	10.4	2.19
14	3.8	11.42	–	< 1

Table 2.1: Δ_{3dB} and Q_{ext} for different dimensions of the aperture when $l_{th} = 0.01$ mm.

ap (mm)	bp (mm)	f_0 (GHz)	Δ_{3dB} (GHz)	Q_{ext}
13	0.2	11.51	0.88	26.16
13.05	0.45	11.51	1.63	14.12
13.1	0.7	11.5	2.26	10.18
13.3	1.7	11.5	4.54	5.07
13.5	2.6	11.54	6.94	3.31
14	3.8	11.56	11.07	2.08

Table 2.2: Δ_{3dB} and Q_{ext} for different dimensions of the aperture when $l_{th} = 1$ mm.

ap (mm)	bp (mm)	f_0 (GHz)	Δ_{3dB} (GHz)	Q_{ext}
13	0.2	11.51	0.52	44.27
13.05	0.45	11.51	1.05	21.92
13.1	0.7	11.5	1.51	15.24
13.3	1.7	11.48	3.49	6.59
13.5	2.6	11.52	5.17	4.45
14	3.8	11.48	9.07	2.54

Table 2.3: Δ_{3dB} and Q_{ext} for different dimensions of the aperture when $l_{th} = 2$ mm.

ap (mm)	bp (mm)	f_0 (GHz)	Δ_{3dB} (GHz)	Q_{ext}
13	0.2	11.51	0.37	62.22
13.05	0.45	11.51	0.78	29.51
13.1	0.7	11.49	1.14	20.19
13.3	1.7	11.49	2.9	7.94
13.5	2.6	11.48	4.13	5.57
14	3.8	11.47	8.84	2.60

Table 2.4: Δ_{3dB} and Q_{ext} for different dimensions of the aperture when $l_{th} = 3$ mm.

ap (mm)	bp (mm)	f_0 (GHz)	Δ_{3dB} (GHz)	Q_{ext}
13	0.2	11.51	0.23	100.09
13.05	0.45	11.5	0.51	45.14
13.1	0.7	11.48	0.76	30.29
13.3	1.7	11.47	2.16	10.66
13.5	2.6	11.47	3.34	6.89
14	3.8	11.47	7.48	3.08

Table 2.5: Δ_{3dB} and Q_{ext} for different dimensions of the aperture when $l_{th} = 5$ mm.

In Fig. 2.8 we can see the variation of the 3 dB bandwidth (Δ_{3dB}) for a filter with a center frequency (f_0) of 11.5 GHz, as a function of the width of the aperture (ap) for different aperture's thickness (l_{th}). Here we can observe that the 3 dB bandwidth (Δ_{3dB}) is directly proportional to the aperture's width and height ($ap \times bp$). However, we observe that this variable decreases when increasing the aperture's thickness (l_{th}).

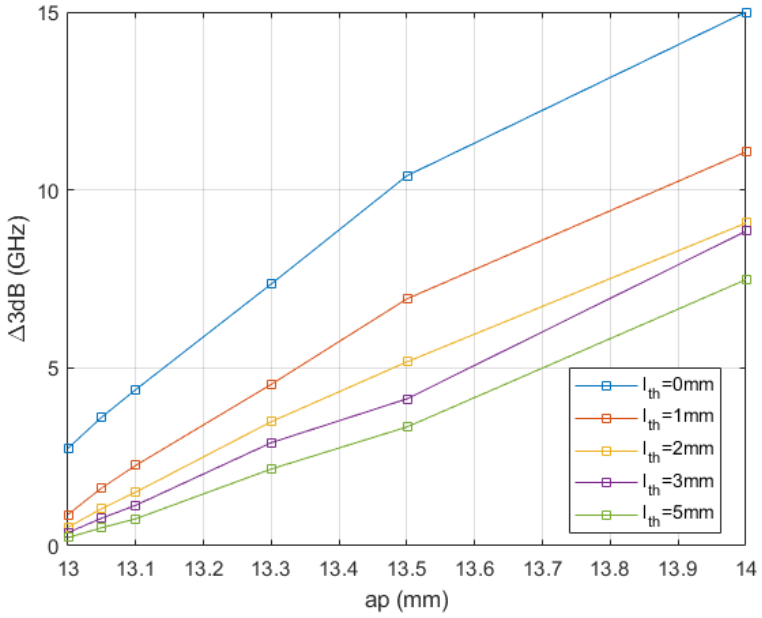

Figure 2.8: Variation of the Δ_{3dB} as a function of ap, for different values of l_{th}.

In Fig. 2.9 we observe the external quality factor as a function of the width of the aperture (ap) for different aperture's thickness (l_{th}).

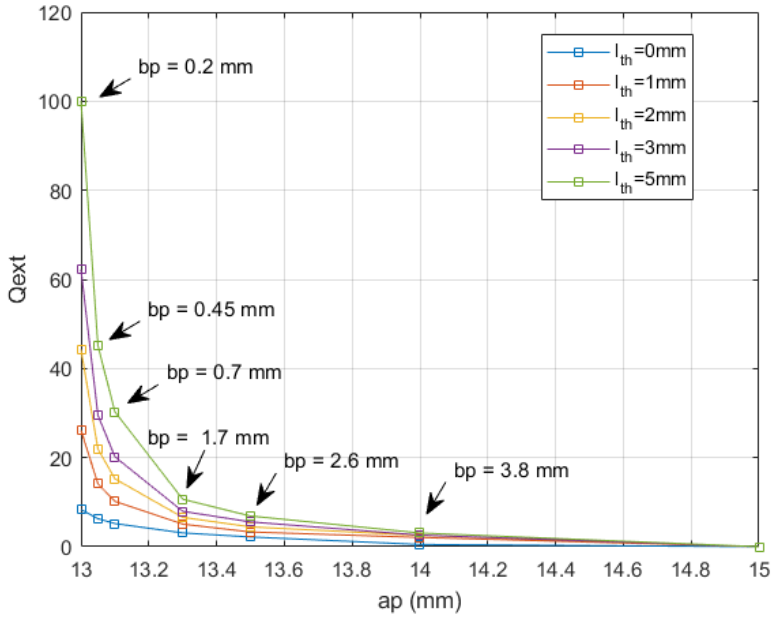

Figure 2.9: Variation of the Q_{ext} as a function of ap, for different values of l_{th}.

In Fig. 2.9 we observe that to increase the external quality factor of the structure, the width (ap) and height (bp) of the aperture must be decreased, leading to a decrease of the input/output coupling. To obtain a low Q_{ext} it is necessary to increase these variables, which will lead to a rise of the input/output coupling. Furthermore, for a fixed height and width, it is possible to increase the external quality factor by increasing the thickness of the aperture (l_{th}).
This behaviour can also be analyzed in terms of input/output coupling. In Fig. 2.5 we can see that the variation of the aperture's width (ap) does not affect significantly the input/output coupling. However, in Fig. 2.6, we observe that the input/output coupling is very sensitive to the height of the aperture (bp), since when decreasing this variable, the coupling also decreases significantly. Finally, in Fig. 2.7, we also observe that the input/output coupling decreases significantly with the increment of the aperture's thickness (l_{th}), meaning that the Q_{ext} increases with this variable, which is the conclusion we also have come to in Fig. 2.9. Therefore, in order to obtain a high Q_{ext}, the aperture must be small. However, as we have already mentioned, a limit of bp=0.2 mm has been set so that the manufacturing of the filter is possible. If we want to increase the external quality factor avoiding small values for the height of the aperture (bp), we also can increase the thickness of the aperture l_{th}.
It can be seen that these filters have a broadband nature, since large bandwidths are obtained. In fact, it is difficult to obtain a bandwidth smaller than 10% of the resonant frequency, and in this case the behaviour of the filter would be very sensitive, which means that small changes of the aperture's width would lead to big drifts in the resonant frequency.

2.4. Unloaded quality factor (Q_u)

The unloaded quality factor (Q_u) is defined as:

$$Q_u = \omega_0 \frac{W_T}{P_{loss}}, \tag{2.4}$$

where w_0 is the radian resonant frequency, W_T is the average energy stored, and P_{loss} is the power dissipated in the resonator [3].
The Q_u is a measure of the loss of the resonator itself, disregarding external loading effects. Resonator losses may be due to conductor loss or dielectric loss [8].
In order to measure the unloaded quality factor (Q_u) for the different resonators in the study, the eigenmode solver has been used. The structure simulated is the same as in the previous study, but now the structure does not have input/output ports. Besides, until now the background of the structure has been PEC (Perfect Electric Conductor), which means that there were no losses in the structure. However, in this case, we need to use a real material in order to measure how well the resonator works. Therefore, we have changed the background of the strucure to Aluminum (σ = 38000000 S/m), as seen in Fig. 2.10.

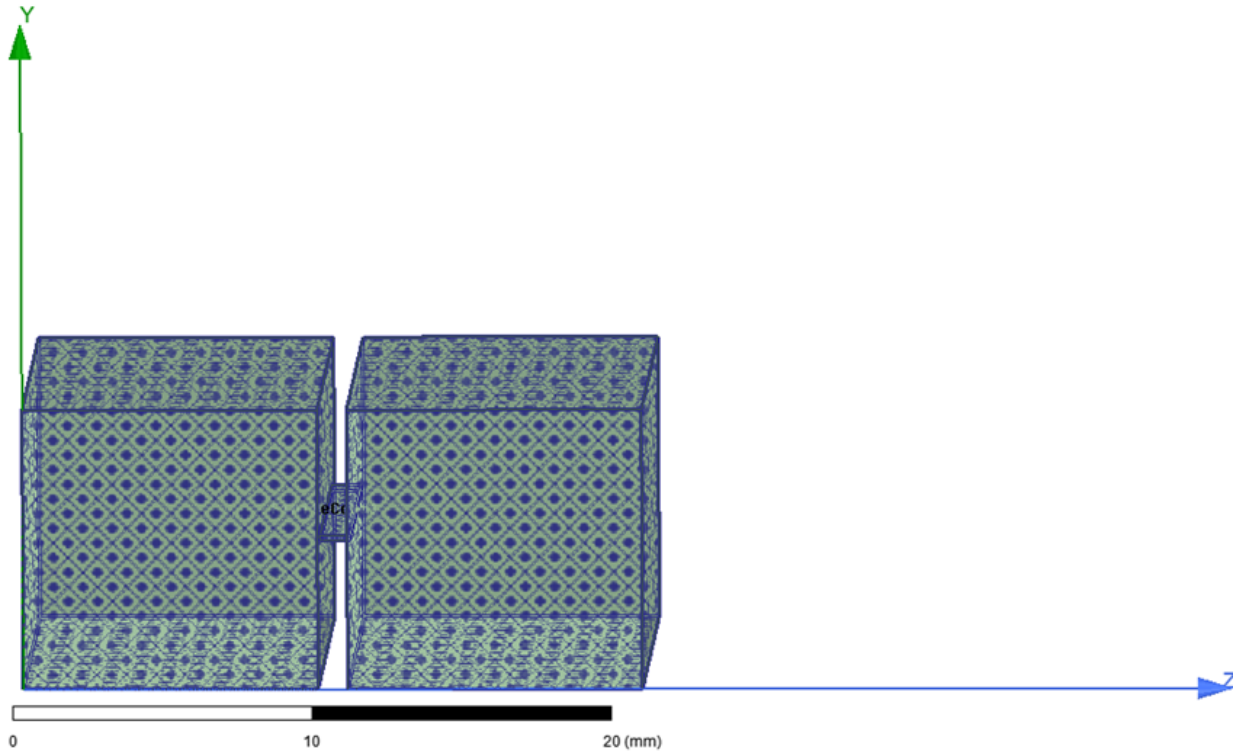

Figure 2.10: Structure under analysis for the Q_u calculation, with Alumimun background (σ = 38000000 S/m) and without input/output ports.

In this case, when using the eigenmode solver, the unloaded quality factor (Q_u) is automatically given by Ansys HFSS [6]. We have performed an analysis for the same sizes of apertures as in the characterization of the Q_{ext}. The results are shown in Tables 2.6 - 2.10.

ap (mm)	bp (mm)	l_{th} (mm)	f_0 (GHz)	Q_u
13	0.2	0.01	11.25	481.36
13.05	0.45	0.01	11.21	859.82
13.1	0.7	0.01	11.20	1064.27
13.3	1.7	0.01	11.14	1874.62
13.5	2.6	0.01	11.13	2210.59
14	3.8	0.01	11.09	2677.31

Table 2.6: Q_u for different dimensions of the aperture when $l_{th} = 0.01$ mm.

ap (mm)	bp (mm)	l_{th} (mm)	f_0 (GHz)	Q_u
13	0.2	1	11.4	314.05
13.05	0.45	1	11.36	692.65
13.1	0.7	1	11.32	1030.65
13.3	1.7	1	11.21	1989.41
13.5	2.6	1	11.17	2559.55
14	3.8	1	11.07	3198.62

Table 2.7: Q_u for different dimensions of the aperture when $l_{th} = 1$ mm.

ap (mm)	bp (mm)	l_{th} (mm)	f_0 (GHz)	Q_u
13	0.2	2	11.46	314.05
13.05	0.45	2	11.41	653.5
13.1	0.7	2	11.36	983.184
13.3	1.7	2	11.23	1974.55
13.5	2.6	2	11.17	2620.6
14	3.8	2	11.03	3265.3

Table 2.8: Q_u for different dimensions of the aperture when $l_{th} = 2$ mm.

ap (mm)	bp (mm)	l_{th} (mm)	f_0 (GHz)	Q_u
13	0.2	3	11.47	280.59
13.05	0.45	3	11.43	629.43
13.1	0.7	3	11.37	954.81
13.3	1.7	3	11.25	2107.6
13.5	2.6	3	11.17	2582.62
14	3.8	3	11.02	3326.66

Table 2.9: Q_u for different dimensions of the aperture when $l_{th} = 3$ mm.

ap (mm)	bp (mm)	l_{th} (mm)	f_0 (GHz)	Q_u
13	0.2	5	11.49	272.74
13.05	0.45	5	11.44	602.21
13.1	0.7	5	11.39	908.94
13.3	1.7	5	11.26	2130.4
13.5	2.6	5	11.17	2672.38
14	3.8	5	10.96	3331

Table 2.10: Q_u for different dimensions of the aperture when $l_{th} = 5$ mm.

In Fig. 2.11, the variation of the unloaded quality factor as a function of the aperture's width (ap) for different aperture's thickness (l_{th}) is shown.

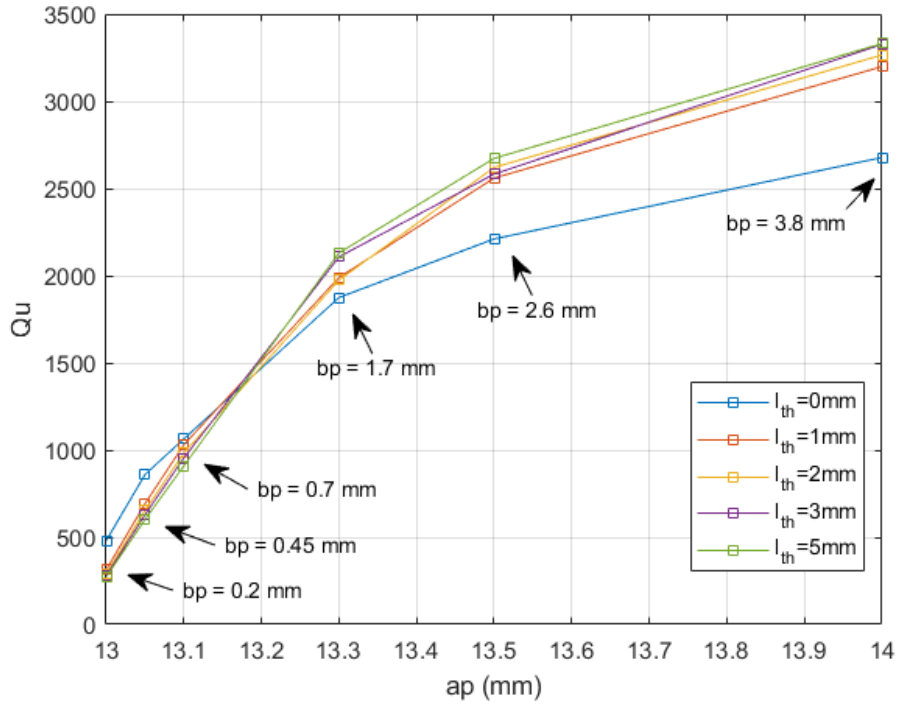

Figure 2.11: Variation of the Q_u as a function of ap for different l_{th}.

It should be noted that in these simulations, the height of the aperture (bp) is adjusted in order to mantain the resonant frequency (f_0) fixed. The unloaded quality factor is directly proportional to the width of the iris (ap). Therefore, as we make the iris bigger, the Q_u increases as well. As we can see in Fig. 2.11, the results are very dependent with the size of the aperture's width and height ($ap \times bp$). The maximum Qu of 3331 is obtained for an aperture size ($ap \times bp \times l_{th}$) of 14 mm $\times$ 3.8 mm $\times$ 5 mm, whereas the minimum of 272.74 has been obtained for an aperture size ($ap \times bp \times l_{th}$) of 13 mm $\times$ 0.2 mm $\times$ 5 mm. Moreover, we can see that in general, higher Q_u are obtained when increasing the thickness of the aperture l_{th}, but we can see a saturation effect from $l_{th} = 3$ mm, since from here the Q_u does not increase significantly. In order to put the results into context, we have collected in Table 2.11 the order of magnitude of the typical Q_u values for different technologies.

Technology	$\approx Q_u$
Microstrip	100 - 200
Waveguide	5000
SIW	300
Resonant apertures	300 - 3000

Table 2.11: Order of magnitude of the typical Q_u values for different technologies.

Therefore, depending on the aplication, if we need to have resonators with high unloaded quality factor (Q_u), we will need to choose big sizes of apertures.

2.5. Inter-resonator coupling (k)

The inter-resonator coupling (k) is defined as the ratio of the energy transferred between two resonators to the energy stored in a resonator [7]. In order to study the inter-resonator coupling (k), we use two symmetric coupled resonators (see Fig. 2.1) and we split this structure in half applying symmetry, leading to the structure shown in Fig. 2.12.

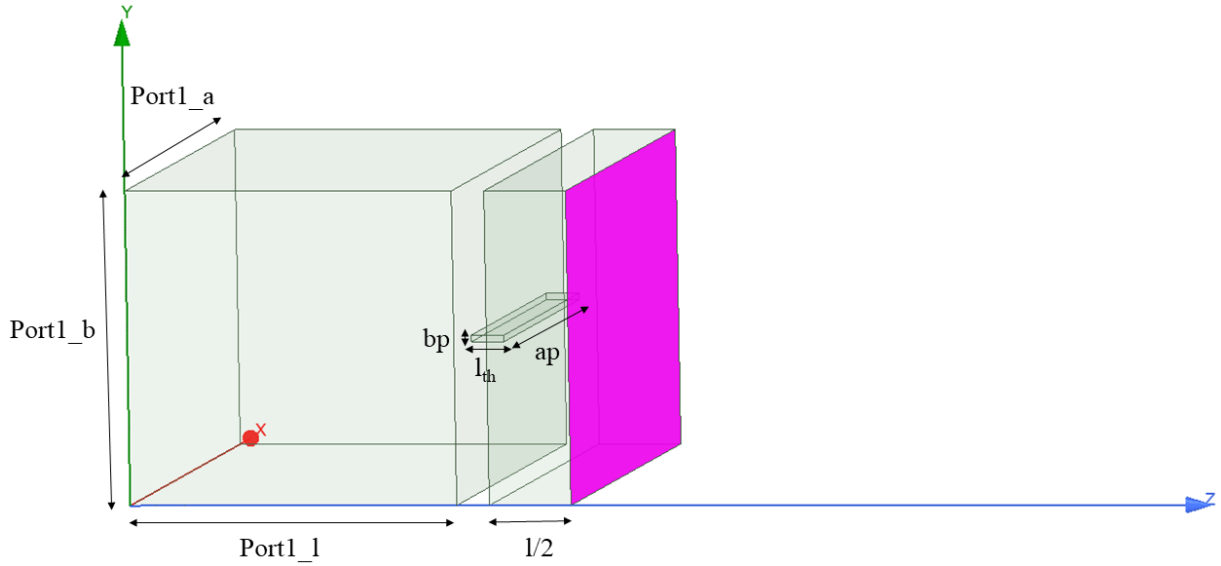

Figure 2.12: Structure simulated to obtain the inter-resonator coupling, applying a symmetry plane (pink surface) to a structure composed of two symmetric coupled resonators.

Then, a magnetic or electric wall is placed in the symmetry plane where the structure was splitted, and an eigenmode analysis is made to determine the magnetic f_m (f_{even}) and electric f_e (f_{odd}) resonant frequencies. Once these two frequencies are obtained, the inter-resonator coupling is computed as explained in [3]:

$$k = \frac{f_e^2 - f_m^2}{f_e^2 + f_m^2} \tag{2.5}$$

In this case, $f_e > f_m$, so the coupling is positive.
We have also calculated the resonant frequency (f_0) in order to see if there is a big drift between the different tests, as follows:

$$f_0 = \frac{f_e + f_m}{2} \tag{2.6}$$

We have performed this test for different lengths of the intermediate waveguide section (l) (see Fig. 2.12) to see how the inter-resonator coupling varies. In the following tables, the intermediate waveguide section (l) is referred to as Int. WG section. This test has been repeated for different sizes ($ap \times bp \times l_{th}$) of the aperture. The obtained results are collected in Tables 2.12 - 2.41 and in Figures 2.13 - 2.18.

Size of the aperture			**Int. WG section**				
ap (mm)	bp (mm)	l_{th} (mm)	l (mm)	f_e (GHz)	f_m (GHz)	f_0 (GHz)	k
13	0.2	0.01	1	14.86	11.29	13.01	0.268
13	0.2	0.01	2	13.64	11.21	12.43	0.193
13	0.2	0.01	3	13.02	11.19	12.10	0.150
13	0.2	0.01	4	12.62	11.14	11.88	0.124
13	0.2	0.01	5	12.28	11.05	11.66	0.106
13	0.2	0.01	7	12.08	10.99	11.53	0.094
13	0.2	0.01	10	11.75	10.79	11.27	0.085

Table 2.12: Inter-resonator coupling as a function of l (mm) for a 13 mm $\times$ 0.2 mm $\times$ 0.01 mm iris.

Size of the aperture			**Int. WG section**				
ap (mm)	bp (mm)	l_{th} (mm)	l (mm)	f_e (GHz)	f_m (GHz)	f_0 (GHz)	k
13	0.2	1	1	13.31	11.43	12.37	0.151
13	0.2	1	2	12.53	11.43	12.03	0.092
13	0.2	1	3	12.20	11.42	11.81	0.066
13	0.2	1	4	12.03	11.41	11.72	0.053
13	0.2	1	5	11.92	11.38	11.65	0.046
13	0.2	1	7	11.77	11.34	11.55	0.037
13	0.2	1	10	11.65	11.26	11.46	0.035

Table 2.13: Inter-resonator coupling as a function of l (mm) for a 13 mm $\times$ 0.2 mm $\times$ 1 mm iris.

Size of the aperture			**Int. WG section**				
ap (mm)	bp (mm)	l_{th} (mm)	l (mm)	f_e (GHz)	f_m (GHz)	f_0 (GHz)	k
13	0.2	2	1	12.72	11.48	12.10	0.102
13	0.2	2	2	12.17	11.47	11.83	0.059
13	0.2	2	3	11.94	11.45	11.69	0.042
13	0.2	2	4	11.82	11.43	11.63	0.033
13	0.2	2	5	11.76	11.45	11.61	0.027
13	0.2	2	7	11.66	11.41	11.53	0.022
13	0.2	2	10	11.60	11.35	11.48	0.022

Table 2.14: Inter-resonator coupling as a function of l (mm) for a 13 mm $\times$ 0.2 mm $\times$ 2 mm iris.

Size of the aperture			**Int. WG section**				
ap (mm)	bp (mm)	l_{th} (mm)	l (mm)	f_e (GHz)	f_m (GHz)	f_0 (GHz)	k
13	0.2	3	1	12.43	11.49	11.96	0.078
13	0.2	3	2	11.99	11.48	11.74	0.044
13	0.2	3	3	11.84	11.48	11.66	0.031
13	0.2	3	4	11.75	11.47	11.61	0.024
13	0.2	3	5	11.69	11.47	11.58	0.019
13	0.2	3	7	11.64	11.45	11.54	0.016
13	0.2	3	10	11.59	11.40	11.49	0.016

Table 2.15: Inter-resonator coupling as a function of l (mm) for a 13 mm $\times$ 0.2 mm $\times$ 3 mm iris.

Size of the aperture			**Int. WG section**				
ap (mm)	bp (mm)	l_{th} (mm)	l (mm)	f_e (GHz)	f_m (GHz)	f_0 (GHz)	k
13	0.2	5	1	12.09	11.51	11.80	0.049
13	0.2	5	2	11.83	11.51	11.69	0.028
13	0.2	5	3	11.73	11.49	11.61	0.019
13	0.2	5	4	11.67	11.49	11.58	0.016
13	0.2	5	5	11.65	11.48	11.57	0.014
13	0.2	5	7	11.59	11.47	11.53	0.010
13	0.2	5	10	11.57	11.45	11.51	0.010

Table 2.16: Inter-resonator coupling as a function of l (mm) for a 13 mm $\times$ 0.2 mm $\times$ 5 mm iris.

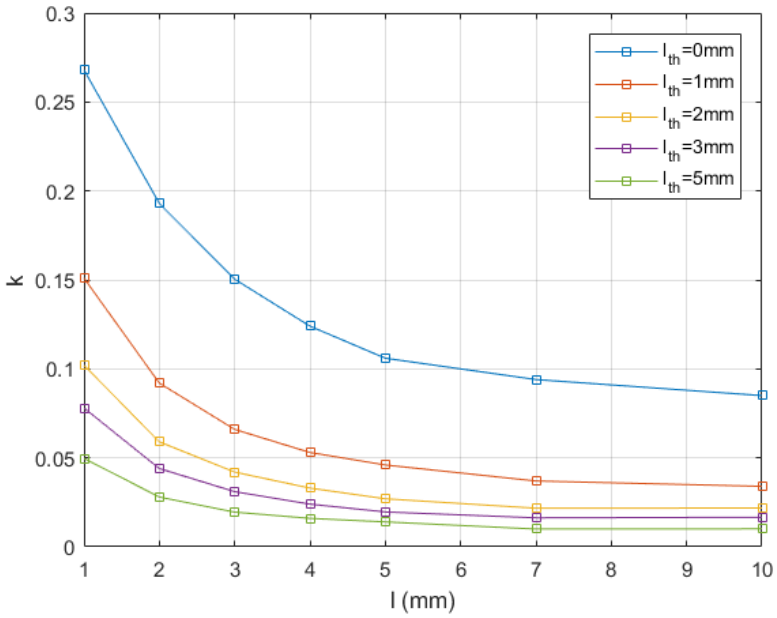

Figure 2.13: Inter-resonator coupling as a function of l (mm) for different l_{th} (mm) for a 13 mm × 0.2 mm iris.

Size of the aperture			**Int. WG section**				
ap (mm)	bp (mm)	l_{th} (mm)	l (mm)	f_e (GHz)	f_m (GHz)	f_0 (GHz)	k
13.05	0.45	0.01	1	15.23	11.24	13.23	0.295
13.05	0.45	0.01	2	14.09	11.18	12.63	0.227
13.05	0.45	0.01	3	13.36	11.11	12.24	0.182
13.05	0.45	0.01	4	12.95	11.05	12.00	0.157
13.05	0.45	0.01	5	12.63	11.02	11.83	0.135
13.05	0.45	0.01	7	12.21	10.89	11.55	0.113
13.05	0.45	0.01	10	11.84	10.71	11.28	0.100

Table 2.17: Inter-resonator coupling as a function of l (mm) for a 13.05 mm × 0.45 mm × 0.01 mm iris.

Size of the aperture			**Int. WG section**				
ap (mm)	bp (mm)	l_{th} (mm)	l (mm)	f_e (GHz)	f_m (GHz)	f_0 (GHz)	k
13.05	0.45	1	1	14.23	11.38	12.81	0.219
13.05	0.45	1	2	13.14	11.34	12.24	0.146
13.05	0.45	1	3	12.63	11.33	11.98	0.108
13.05	0.45	1	4	12.34	11.29	11.82	0.089
13.05	0.45	1	5	12.15	11.26	11.71	0.076
13.05	0.45	1	7	11.92	11.19	11.56	0.063
13.05	0.45	1	10	11.71	11.07	11.39	0.056

Table 2.18: Inter-resonator coupling as a function of l (mm) for a 13.05 mm × 0.45 mm × 1 mm iris.

Size of the aperture			**Int. WG section**				
ap (mm)	bp (mm)	l_{th} (mm)	l (mm)	f_e (GHz)	f_m (GHz)	f_0 (GHz)	k
13.05	0.45	2	1	13.53	11.42	12.48	0.168
13.05	0.45	2	2	12.65	11.39	12.02	0.104
13.05	0.45	2	3	12.28	11.38	11.83	0.076
13.05	0.45	2	4	12.08	11.37	11.72	0.060
13.05	0.45	2	5	11.94	11.33	11.64	0.053
13.05	0.45	2	7	11.79	11.29	11.54	0.043
13.05	0.45	2	10	11.64	11.20	11.42	0.039

Table 2.19: Inter-resonator coupling as a function of l (mm) for a 13.05 mm $\times$ 0.45 mm $\times$ 2 mm iris.

Size of the aperture			**Int. WG section**				
ap (mm)	bp (mm)	l_{th} (mm)	l (mm)	f_e (GHz)	f_m (GHz)	f_0 (GHz)	k
13.05	0.45	3	1	13.09	11.44	12.27	0.134
13.05	0.45	3	2	12.39	11.43	12.91	0.081
13.05	0.45	3	3	12.09	11.40	11.71	0.058
13.05	0.45	3	4	11.94	11.39	11.67	0.047
13.05	0.45	3	5	11.84	11.38	11.61	0.039
13.05	0.45	3	7	11.72	11.34	11.53	0.033
13.05	0.45	3	10	11.61	11.26	11.44	0.030

Table 2.20: Inter-resonator coupling as a function of l (mm) for a 13.05 mm $\times$ 0.45 mm $\times$ 3 mm iris.

Size of the aperture			**Int. WG section**				
ap (mm)	bp (mm)	l_{th} (mm)	l (mm)	f_e (GHz)	f_m (GHz)	f_0 (GHz)	k
13.05	0.45	5	1	12.58	11.46	12.02	0.093
13.05	0.45	5	2	12.08	11.44	11.76	0.055
13.05	0.45	5	3	11.89	11.43	11.66	0.039
13.05	0.45	5	4	11.79	11.43	11.61	0.031
13.05	0.45	5	5	11.72	11.41	11.57	0.027
13.05	0.45	5	7	11.64	11.39	11.52	0.022
13.05	0.45	5	10	11.57	11.33	11.45	0.021

Table 2.21: Inter-resonator coupling as a function of l (mm) for a 13.05 mm $\times$ 0.45 mm $\times$ 5 mm iris.

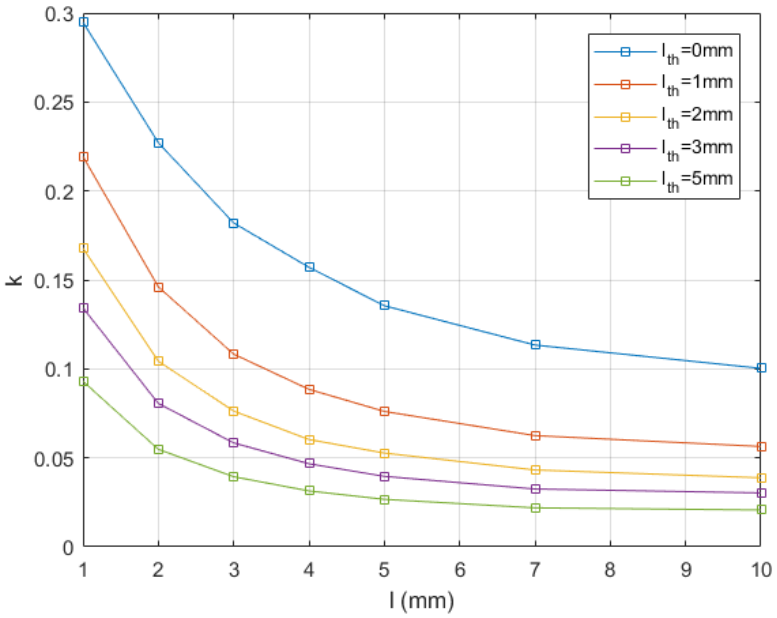

Figure 2.14: Inter-resonator coupling as a function of l (mm) for different l_{th} (mm) for a 13.05 mm × 0.45 mm iris.

Size of the aperture			**Int. WG section**				
ap (mm)	bp (mm)	l_{th} (mm)	l (mm)	f_e (GHz)	f_m (GHz)	f_0 (GHz)	k
13.1	0.7	0.01	1	15.39	11.21	13.29	0.307
13.1	0.7	0.01	2	14.30	11.12	12.71	0.247
13.1	0.7	0.01	3	13.57	11.05	12.31	0.203
13.1	0.7	0.01	4	13.11	10.99	12.05	0.174
13.1	0.7	0.01	5	12.75	10.93	11.84	0.153
13.1	0.7	0.01	7	12.29	10.78	11.54	0.131
13.1	0.7	0.01	10	11.90	10.59	11.25	0.116

Table 2.22: Inter-resonator coupling as a function of l (mm) for a 13.1 mm × 0.7 mm × 0.01 mm iris.

Size of the aperture			**Int. WG section**				
ap (mm)	bp (mm)	l_{th} (mm)	l (mm)	f_e (GHz)	f_m (GHz)	f_0 (GHz)	k
13.1	0.7	1	1	14.66	11.34	12.99	0.251
13.1	0.7	1	2	13.51	11.29	12.40	0.177
13.1	0.7	1	3	12.92	11.25	12.08	0.137
13.1	0.7	1	4	12.57	11.22	11.89	0.113
13.1	0.7	1	5	12.33	11.18	11.76	0.098
13.1	0.7	1	7	12.02	11.09	11.55	0.080
13.1	0.7	1	10	11.76	10.93	11.35	0.073

Table 2.23: Inter-resonator coupling as a function of l (mm) for a 13.1 mm × 0.7 mm × 1 mm iris.

Size of the aperture			**Int. WG section**				
ap (mm)	bp (mm)	l_{th} (mm)	l (mm)	f_e (GHz)	f_m (GHz)	f_0 (GHz)	k
13.1	0.7	2	1	14.00	11.37	12.69	0.205
13.1	0.7	2	2	12.99	11.34	12.17	0.135
13.1	0.7	2	3	12.53	11.32	11.92	0.101
13.1	0.7	2	4	12.26	11.28	11.77	0.083
13.1	0.7	2	5	12.09	11.26	11.67	0.071
13.1	0.7	2	7	11.87	11.19	11.53	0.058
13.1	0.7	2	10	11.68	11.07	11.37	0.054

Table 2.24: Inter-resonator coupling as a function of l (mm) for a 13.1 mm $\times$ 0.7 mm $\times$ 2 mm iris.

Size of the aperture			**Int. WG section**				
ap (mm)	bp (mm)	l_{th} (mm)	l (mm)	f_e (GHz)	f_m (GHz)	f_0 (GHz)	k
13.1	0.7	3	1	13.51	11.39	12.45	0.169
13.1	0.7	3	2	12.67	11.37	12.02	0.108
13.1	0.7	3	3	12.29	11.35	11.82	0.080
13.1	0.7	3	4	12.08	11.32	11.70	0.065
13.1	0.7	3	5	11.94	11.29	11.62	0.055
13.1	0.7	3	7	11.77	11.25	11.51	0.046
13.1	0.7	3	10	11.63	11.15	11.39	0.042

Table 2.25: Inter-resonator coupling as a function of l (mm) for a 13.1 mm $\times$ 0.7 mm $\times$ 3 mm iris.

Size of the aperture			**Int. WG section**				
ap (mm)	bp (mm)	l_{th} (mm)	l (mm)	f_e (GHz)	f_m (GHz)	f_0 (GHz)	k
13.1	0.7	5	1	12.88	11.41	12.14	0.121
13.1	0.7	5	2	12.29	11.39	11.84	0.075
13.1	0.7	5	3	12.03	11.37	11.70	0.056
13.1	0.7	5	4	11.88	11.36	11.62	0.045
13.1	0.7	5	5	11.79	11.34	11.57	0.038
13.1	0.7	5	7	11.67	11.31	11.49	0.032
13.1	0.7	5	10	11.57	11.23	11.40	0.030

Table 2.26: Inter-resonator coupling as a function of l (mm) for a 13.1 mm $\times$ 0.7 mm $\times$ 5 mm iris.

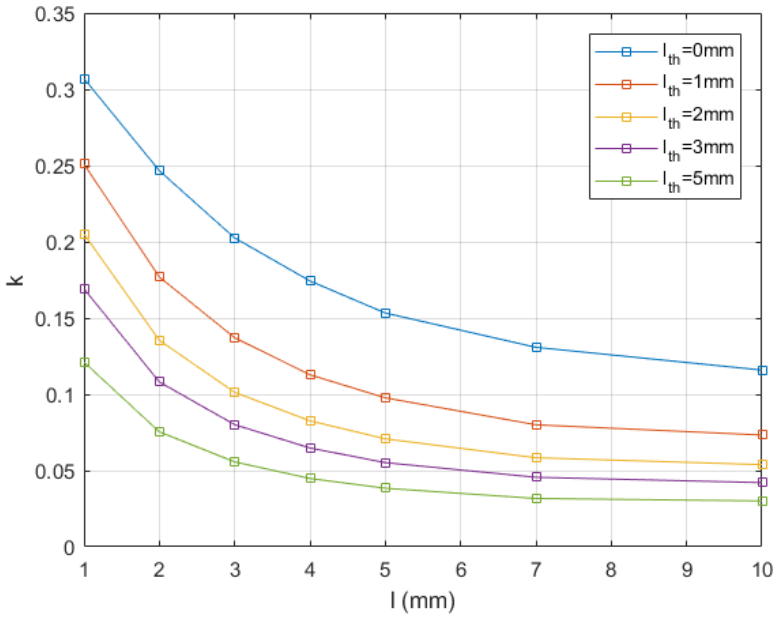

Figure 2.15: Inter-resonator coupling as a function of l (mm) for different l_{th} (mm) for a 13.1 mm × 0.7 mm iris.

Size of the aperture			**Int. WG section**				
ap (mm)	bp (mm)	l_{th} (mm)	l (mm)	f_e (GHz)	f_m (GHz)	f_0 (GHz)	k
13.3	1.7	0.01	1	15.76	11.12	11.12	0.335
13.3	1.7	0.01	2	14.82	11.02	11.02	0.288
13.3	1.7	0.01	3	14.11	11.91	10.91	0.251
13.3	1.7	0.01	4	13.59	11.82	10.82	0.225
13.3	1.7	0.01	5	13.19	11.74	10.74	0.203
13.3	1.7	0.01	7	12.60	10.59	10.59	0.172
13.3	1.7	0.01	10	11.06	10.32	10.32	0.154

Table 2.27: Inter-resonator coupling as a function of l (mm) for a 13.3 mm × 1.7 mm × 0.01 mm iris.

Size of the aperture			**Int. WG section**				
ap (mm)	bp (mm)	l_{th} (mm)	l (mm)	f_e (GHz)	f_m (GHz)	f_0 (GHz)	k
13.3	1.7	1	1	15.30	11.21	13.25	0.302
13.3	1.7	1	2	14.26	11.15	12.71	0.242
13.3	1.7	1	3	13.58	11.08	12.33	0.201
13.3	1.7	1	4	13.11	11.01	12.06	0.172
13.3	1.7	1	5	12.79	10.96	11.87	0.153
13.3	1.7	1	7	12.32	10.83	11.57	0.129
13.3	1.7	1	10	11.91	10.61	11.26	0.116

Table 2.28: Inter-resonator coupling as a function of l (mm) for a 13.3 mm × 1.7 mm × 1 mm iris.

Size of the aperture			**Int. WG section**				
ap (mm)	bp (mm)	l_{th} (mm)	l (mm)	f_e (GHz)	f_m (GHz)	f_0 (GHz)	k
13.3	1.7	2	1	14.78	11.23	13.00	0.268
13.3	1.7	2	2	13.74	11.18	12.46	0.204
13.3	1.7	2	3	13.14	11.14	12.14	0.164
13.3	1.7	2	4	12.75	11.08	11.91	0.139
13.3	1.7	2	5	12.47	11.03	11.75	0.122
13.3	1.7	2	7	12.12	10.93	11.52	0.103
13.3	1.7	2	10	11.79	10.73	11.26	0.094

Table 2.29: Inter-resonator coupling as a function of l (mm) for a 13.3 mm × 1.7 mm × 2 mm iris.

Size of the aperture			**Int. WG section**				
ap (mm)	bp (mm)	l_{th} (mm)	l (mm)	f_e (GHz)	f_m (GHz)	f_0 (GHz)	k
13.3	1.7	3	1	14.27	11.24	12.75	0.234
13.3	1.7	3	2	13.34	11.20	12.27	0.173
13.3	1.7	3	3	12.82	11.16	11.99	0.138
13.3	1.7	3	4	12.45	11.12	11.78	0.113
13.3	1.7	3	5	12.27	11.08	11.67	0.102
13.3	1.7	3	7	11.97	10.98	11.47	0.086
13.3	1.7	3	10	11.71	10.82	11.26	0.079

Table 2.30: Inter-resonator coupling as a function of l (mm) for a 13.3 mm × 1.7 mm × 3 mm iris.

Size of the aperture			**Int. WG section**				
ap (mm)	bp (mm)	l_{th} (mm)	l (mm)	f_e (GHz)	f_m (GHz)	f_0 (GHz)	k
13.3	1.7	5	1	13.44	11.25	12.34	0.177
13.3	1.7	5	2	12.76	11.22	11.99	0.128
13.3	1.7	5	3	12.39	11.19	11.79	0.101
13.3	1.7	5	4	12.15	11.16	11.66	0.085
13.3	1.7	5	5	11.99	11.13	11.56	0.075
13.3	1.7	5	7	11.78	11.05	11.42	0.064
13.3	1.7	5	10	11.59	10.92	11.25	0.059

Table 2.31: Inter-resonator coupling as a function of l (mm) for a 13.3 mm × 1.7 mm × 5 mm iris.

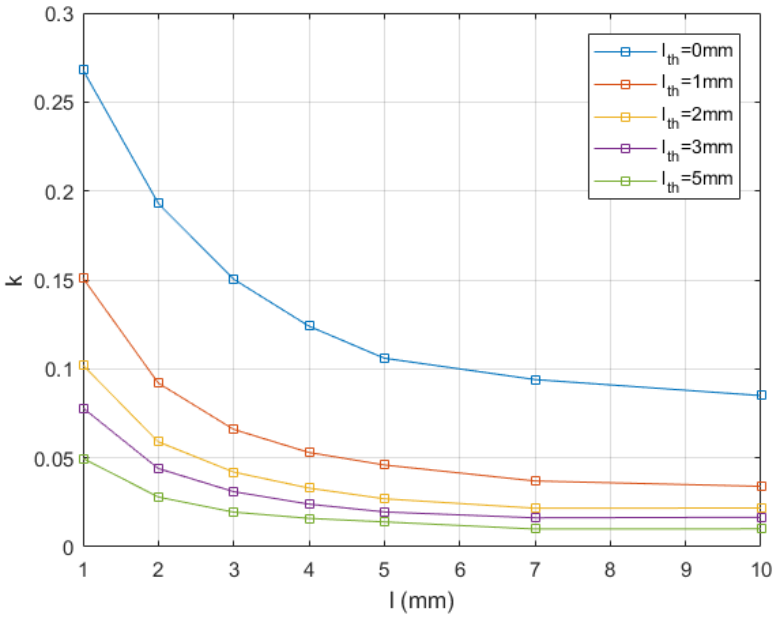

Figure 2.16: Inter-resonator coupling as a function of l (mm) for different l_{th} (mm) for a 13.3 mm × 1.7 mm iris.

Size of the aperture			**Int. WG section**				
ap (mm)	bp (mm)	l_{th} (mm)	l (mm)	f_e (GHz)	f_m (GHz)	f_0 (GHz)	k
13.5	2.6	0.01	1	15.98	11.11	12.54	0.348
13.5	2.6	0.01	2	15.16	10.99	13.07	0.311
13.5	2.6	0.01	3	14.49	10.89	12.69	0.278
13.5	2.6	0.01	4	13.96	10.79	12.37	0.252
13.5	2.6	0.01	5	13.52	10.68	12.10	0.231
13.5	2.6	0.01	7	12.89	10.50	11.69	0.202
13.5	2.6	0.01	10	12.27	10.21	11.24	0.182

Table 2.32: Inter-resonator coupling as a function of l (mm) for a 13.5 mm × 2.6 mm × 0.01 mm iris.

Size of the aperture			**Int. WG section**				
ap (mm)	bp (mm)	l_{th} (mm)	l (mm)	f_e (GHz)	f_m (GHz)	f_0 (GHz)	k
13.5	2.6	1	1	15.50	11.14	13.32	0.319
13.5	2.6	1	2	14.60	11.07	12.83	0.269
13.5	2.6	1	3	13.93	10.99	12.46	0.233
13.5	2.6	1	4	13.45	10.91	12.18	0.206
13.5	2.6	1	5	13.07	10.83	11.95	0.186
13.5	2.6	1	7	12.55	10.68	11.61	0.161
13.5	2.6	1	10	12.05	10.42	11.24	0.144

Table 2.33: Inter-resonator coupling as a function of l (mm) for a 13.5 mm × 2.6 mm × 1 mm iris.

Size of the aperture			**Int. WG section**				
ap (mm)	bp (mm)	l_{th} (mm)	l (mm)	f_e (GHz)	f_m (GHz)	f_0 (GHz)	k
13.5	2.6	2	1	14.99	11.13	13.06	0.289
13.5	2.6	2	2	14.08	11.08	12.58	0.235
13.5	2.6	2	3	13.47	11.02	12.25	0.198
13.5	2.6	2	4	13.05	10.96	12.00	0.173
13.5	2.6	2	5	12.74	10.89	11.81	0.159
13.5	2.6	2	7	12.30	10.76	11.53	0.133
13.5	2.6	2	10	11.89	10.53	11.21	0.121

Table 2.34: Inter-resonator coupling as a function of l (mm) for a 13.5 mm × 2.6 mm × 2 mm iris.

Size of the aperture			**Int. WG section**				
ap (mm)	bp (mm)	l_{th} (mm)	l (mm)	f_e (GHz)	f_m (GHz)	f_0 (GHz)	k
13.5	2.6	3	1	14.46	11.13	12.79	0.256
13.5	2.6	3	2	13.64	11.09	12.36	0.204
13.5	2.6	3	3	13.11	11.04	12.07	0.170
13.5	2.6	3	4	12.74	10.98	11.86	0.148
13.5	2.6	3	5	12.48	10.93	11.70	0.132
13.5	2.6	3	7	12.11	10.81	11.46	0.113
13.5	2.6	3	10	11.77	10.61	11.19	0.104

Table 2.35: Inter-resonator coupling as a function of l (mm) for a 13.5 mm × 2.6 mm × 3 mm iris.

Size of the aperture			**Int. WG section**				
ap (mm)	bp (mm)	l_{th} (mm)	l (mm)	f_e (GHz)	f_m (GHz)	f_0 (GHz)	k
13.5	2.6	5	1	13.58	11.13	12.36	0.197
13.5	2.6	5	2	13.00	11.09	12.05	0.157
13.5	2.6	5	3	12.63	11.06	11.84	0.132
13.5	2.6	5	4	12.37	11.01	11.69	0.115
13.5	2.6	5	5	12.17	10.97	11.57	0.104
13.5	2.6	5	7	11.90	10.87	11.39	0.091
13.5	2.6	5	10	11.65	10.69	11.17	0.086

Table 2.36: Inter-resonator coupling as a function of l (mm) for a 13.5 mm × 2.6 mm × 5 mm iris.

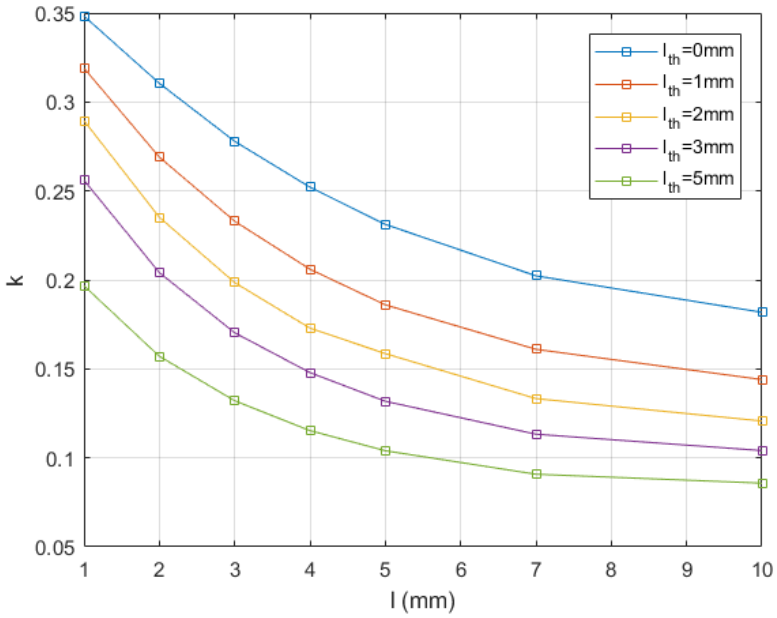

Figure 2.17: Inter-resonator coupling as a function of l (mm) for different l_{th} (mm) for a 13.5 mm × 2.6 mm iris.

Size of the aperture			**Int. WG section**				
ap (mm)	bp (mm)	l_{th} (mm)	l (mm)	f_e (GHz)	f_m (GHz)	f_0 (GHz)	k
14	3.8	0.01	1	16.14	11.02	13.58	0.364
14	3.8	0.01	2	15.42	10.89	13.16	0.333
14	3.8	0.01	3	14.79	10.77	12.78	0.307
14	3.8	0.01	4	14.27	10.65	12.46	0.285
14	3.8	0.01	5	13.83	10.53	12.18	0.266
14	3.8	0.01	7	13.14	10.31	11.73	0.238
14	3.8	0.01	10	12.42	10.00	11.21	0.214

Table 2.37: Inter-resonator coupling as a function of l (mm) for a 14 mm × 3.8 mm × 0.01 mm iris.

Size of the aperture			**Int. WG section**				
ap (mm)	bp (mm)	l_{th} (mm)	l (mm)	f_e (GHz)	f_m (GHz)	f_0 (GHz)	k
14	3.8	1	1	15.58	10.98	13.28	0.336
14	3.8	1	2	14.83	10.88	12.86	0.299
14	3.8	1	3	14.21	10.79	12.50	0.268
14	3.8	1	4	13.72	10.70	12.21	0.243
14	3.8	1	5	13.33	10.60	11.96	0.225
14	3.8	1	7	12.74	10.43	11.58	0.198
14	3.8	1	10	12.15	10.15	11.15	0.178

Table 2.38: Inter-resonator coupling as a function of l (mm) for a 14 mm × 3.8 mm × 1 mm iris.

Size of the aperture			**Int. WG section**				
ap (mm)	bp (mm)	l_{th} (mm)	l (mm)	f_e (GHz)	f_m (GHz)	f_0 (GHz)	k
14	3.8	2	1	15.00	10.93	12.97	0.306
14	3.8	2	2	14.26	10.86	12.56	0.266
14	3.8	2	3	13.69	10.79	12.24	0.234
14	3.8	2	4	13.26	10.71	11.99	0.210
14	3.8	2	5	12.92	10.63	11.78	0.193
14	3.8	2	7	12.43	10.48	11.45	0.169
14	3.8	2	10	11.94	10.22	11.02	0.153

Table 2.39: Inter-resonator coupling as a function of l (mm) for a 14 mm $\times$ 3.8 mm $\times$ 2 mm iris.

Size of the aperture			**Int. WG section**				
ap (mm)	bp (mm)	l_{th} (mm)	l (mm)	f_e (GHz)	f_m (GHz)	f_0 (GHz)	k
14	3.8	3	1	14.43	11.13	12.79	0.256
14	3.8	3	2	13.64	11.09	12.36	0.204
14	3.8	3	3	13.11	11.04	12.07	0.170
14	3.8	3	4	12.74	10.98	11.86	0.148
14	3.8	3	5	12.48	10.93	11.70	0.132
14	3.8	3	7	12.11	10.81	11.46	0.113
14	3.8	3	10	11.77	10.61	11.19	0.104

Table 2.40: Inter-resonator coupling as a function of l (mm) for a 14 mm $\times$ 3.8 mm $\times$ 3 mm iris.

Size of the aperture			**Int. WG section**				
ap (mm)	bp (mm)	l_{th} (mm)	l (mm)	f_e (GHz)	f_m (GHz)	f_0 (GHz)	k
14	3.8	5	1	13.46	10.85	12.15	0.213
14	3.8	5	2	12.97	10.81	11.89	0.181
14	3.8	5	3	12.62	10.76	11.69	0.158
14	3.8	5	4	12.35	10.71	11.53	0.141
14	3.8	5	5	12.14	10.66	11.39	0.129
14	3.8	5	7	11.83	10.54	11.19	0.115
14	3.8	5	10	11.53	10.34	10.94	0.108

Table 2.41: Inter-resonator coupling as a function of l (mm) for a 14 mm $\times$ 3.8 mm $\times$ 5 mm iris.

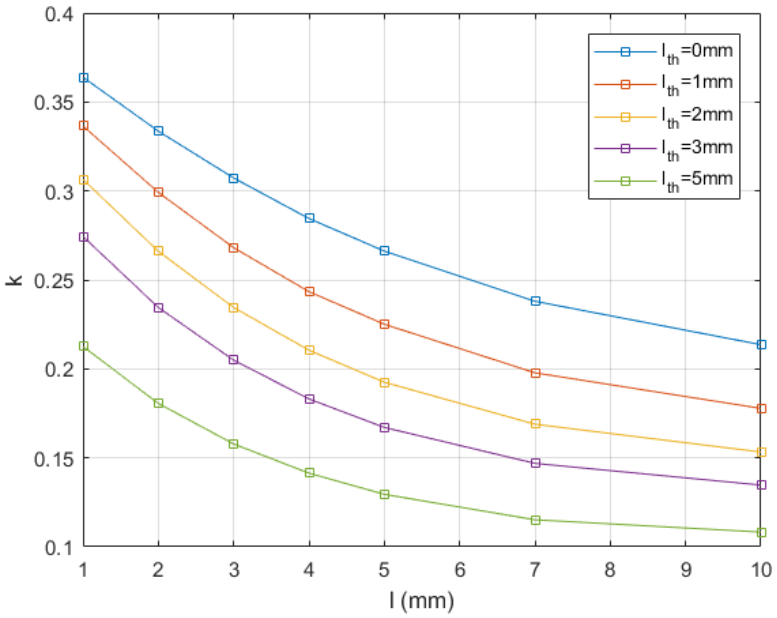

Figure 2.18: Inter-resonator coupling as a function of l (mm) for different l_{th} (mm) for a 14 mm $\times$ 3.8 mm iris.

As we can observe in Fig. 2.13 - 2.18, we obtain a lower inter-resonator coupling (k) when we increase the distance between resonators (l). However we observe a saturation effect in the inter-resonator coupling when increasing l. In order to obtain lower values of k, we also can increase the thickness of the aperture (l_{th}).

2.5.1. Comparative between inter-resonator coupling (k) for the different sizes of apertures.

In this subsection we can see the comparative between the different inter-resonator couplings we have obtained for each size of aperture:

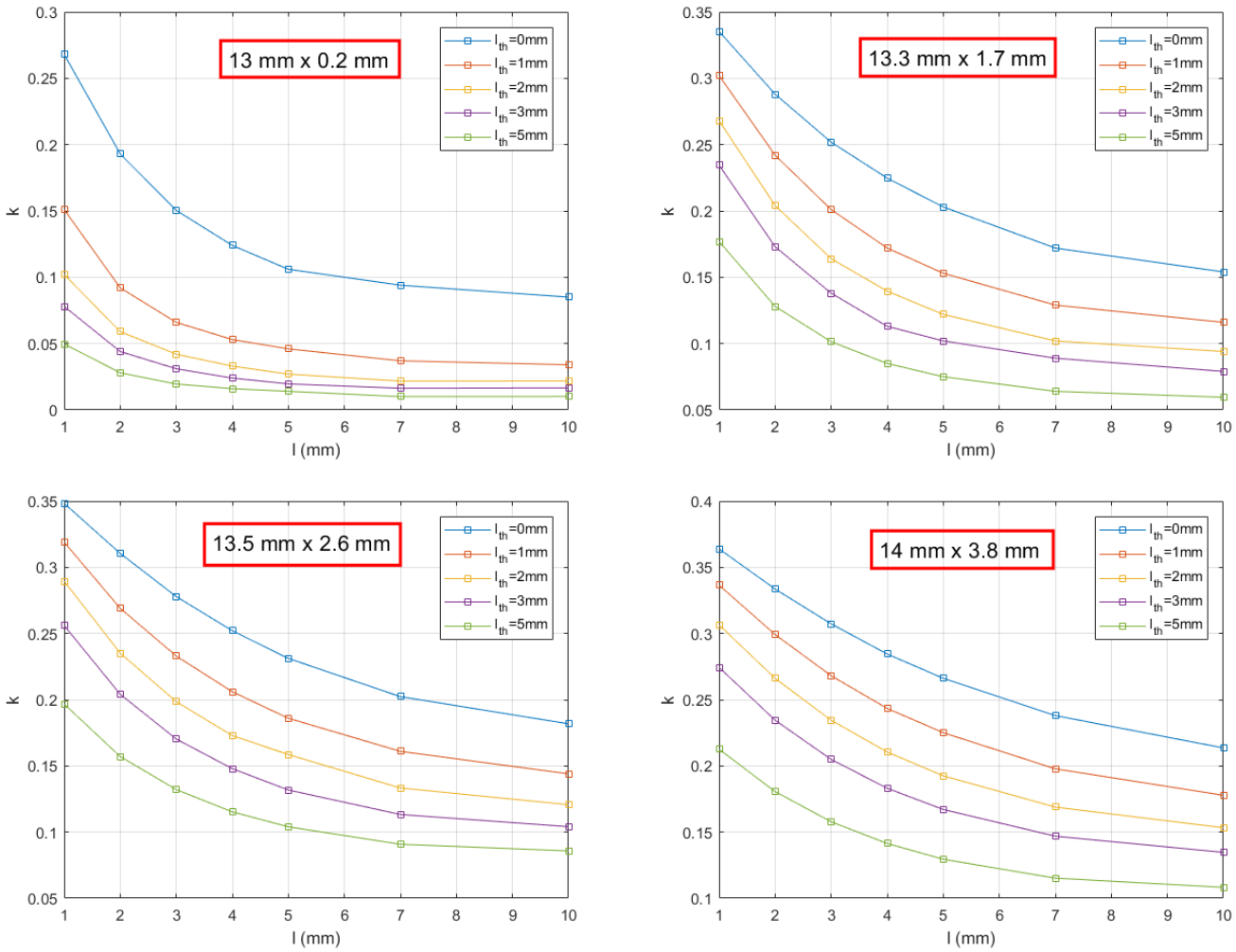

Figure 2.19: Inter-resonator coupling for the resonant aperture's dimensions under study.

As we can see in Fig. 2.19, there are not big differences in the range of values for the inter-resonator coupling (k) that can be obtained with the different aperture's sizes. This will make easier the design of the filters, as we will be able to obtain the same coupling value with different apertures. However, we can observe that for the same length of the intermediate waveguide section (l), the inter-resonator couplings are higher when the aperture is bigger. For example, for a distance between resonators l= 1 mm and a thickness of the aperture l_{th}= 5 mm we obtain a k= 0.05 for an aperture of size 13 mm × 0.2 mm, whereas for an aperture of size 14 mm × 3.8 mm we obtain an inter-resonator coupling k= 0.21.

2.6. Transmission zeros (TZ)

In filter design there is sometimes very restrictive out of band rejection requirements, as we have discussed in Chapter 1. To achieve these requirements, filters with more complex topologies are synthesized. In particular, extracted poles or cross-couplings [3] are normally implemented to obtain transmission zeros in the filter response. In this project, in order to obtain transmission zeros, we have added a step discontinuity between the source and the resonator and between the resonator and the load, so that the symmetry is mantained. This geometry, shown in Fig. 2.20, implements two extracted poles, produced by the excitation of TM_{110} modes in the formed cavities. This implies two transmission zeros in the filter response.

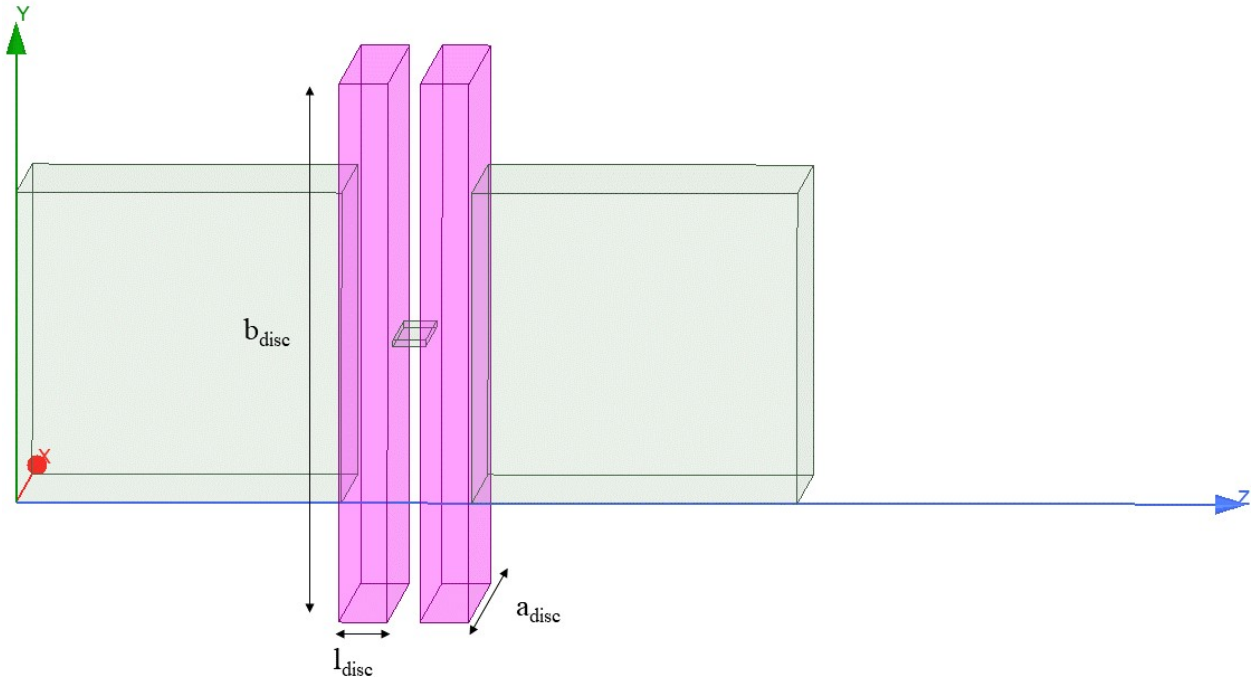

Figure 2.20: Structure under analysis with step discontinuities to implement transmission zeros.

In this way, as we can observe in Fig. 2.21, two almost coincident transmission zeros appear above the passband. To show how to control the position of the two transmission zeros, we plot in Fig. 2.21 the filter response for three different thickness of the step (l_{disc}) while mantaining the width and the height of the step ($a_{disc} \times b_{disc}$) fixed to 28.05 mm $\times$ 18.525 mm.

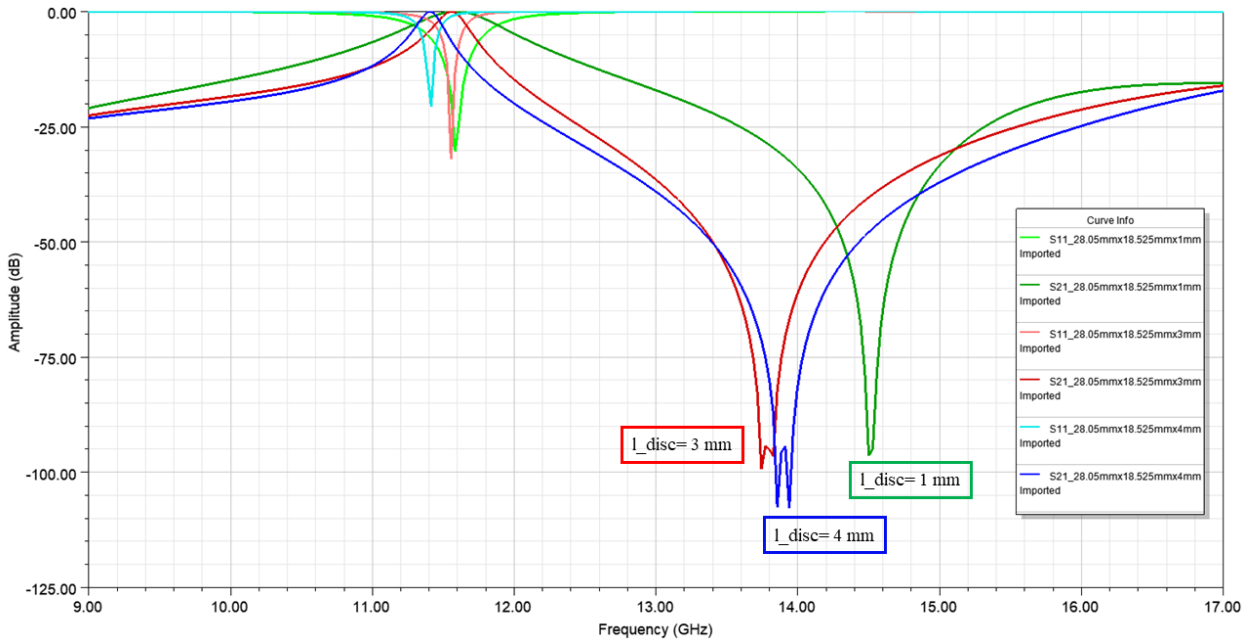

Figure 2.21: S parameters response for the filter in Fig. 2.21 for two different l_{disc} values.

As we can see in Fig. 2.21, if we keep fixed the width and height of the step (a_{disc} and b_{disc}) and vary its length along z-direction (l_{disc}), we observe that when this variable is increased, the frequency position of the transmission zeros decreases. However, we observe a saturation effect if we increase l_{disc} over 3 mm. This can be because the excited modes are TM_{110}, and therefore this drift in the frequency of the transmission zeros is due to the interaction between the formed cavity in the step discontinuity and the aperture.
Now we mantain the length of the step (l_{disc}) fixed to 1.5 mm and make an analysis for different widths and heights of the step. The results of this test are reported in Fig. 2.22.

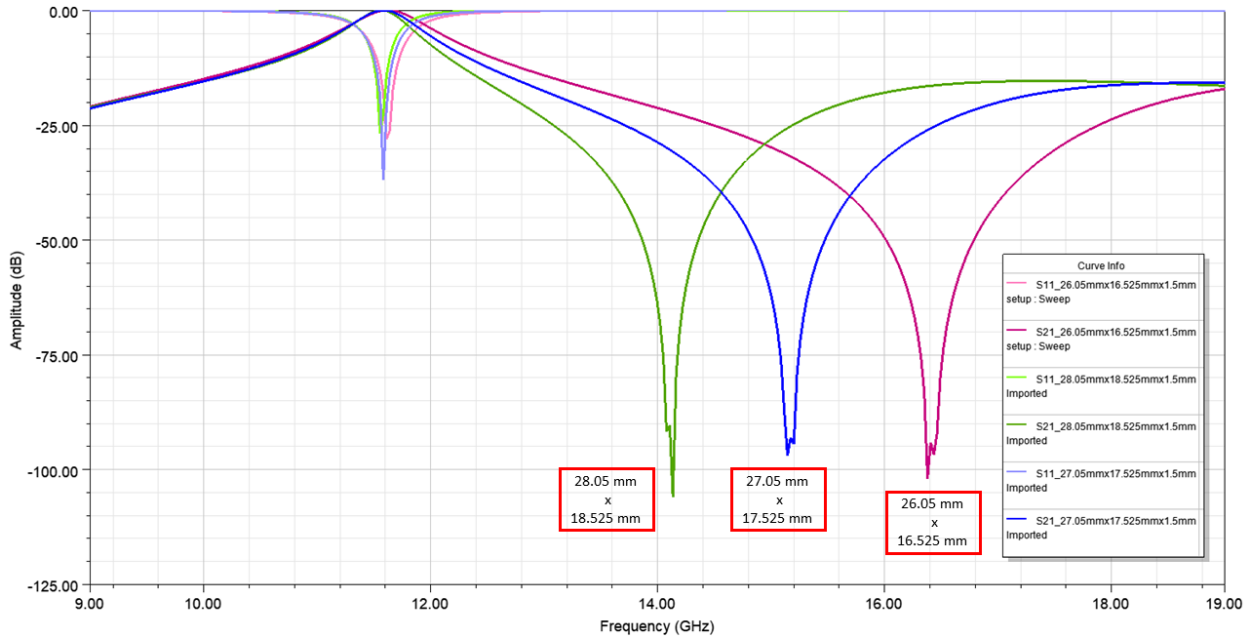

Figure 2.22: S parameters response of the filter in Fig. 2.21 for different widths and heights of the step while keeping constant $l_{disc} = 1.5$ mm.

In this case we can observe that the bigger we make the step discontinuity, the lower the frequency of the transmission zeros is. These transmission zeros could also be controlled independently from each other if desired, by simply changing the dimensions of the input and output discontinuities, but it should be noted that, in this case, the filter would no longer be symmetric, as seen in Fig. 2.23.

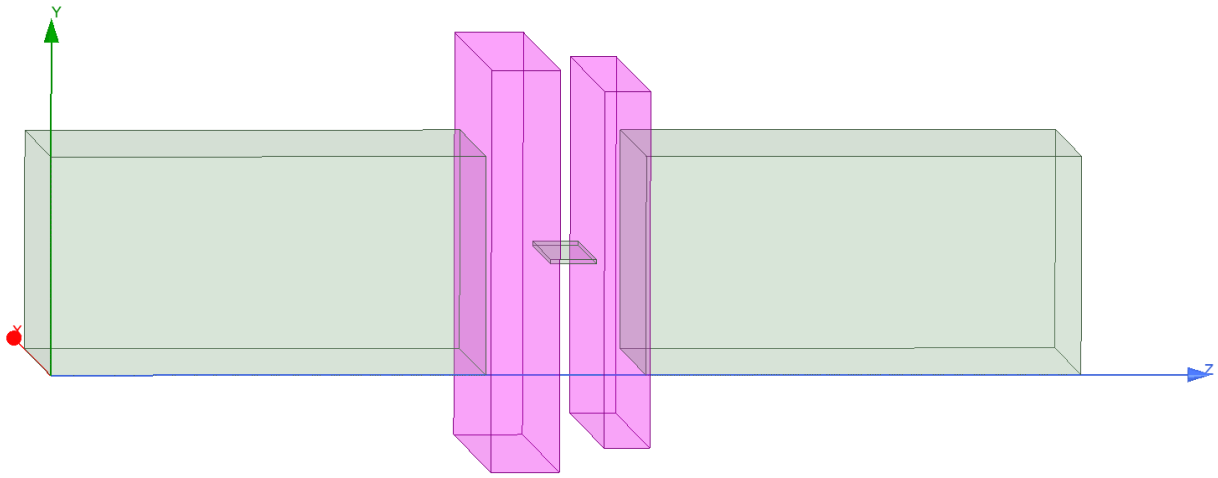

Figure 2.23: Asymmetric structure for the independent control of the two transmission zeros.

In Fig. 2.24 we can see how the resonant frequency of the two transmission zeros is controlled with the dimensions of the discontinuities:

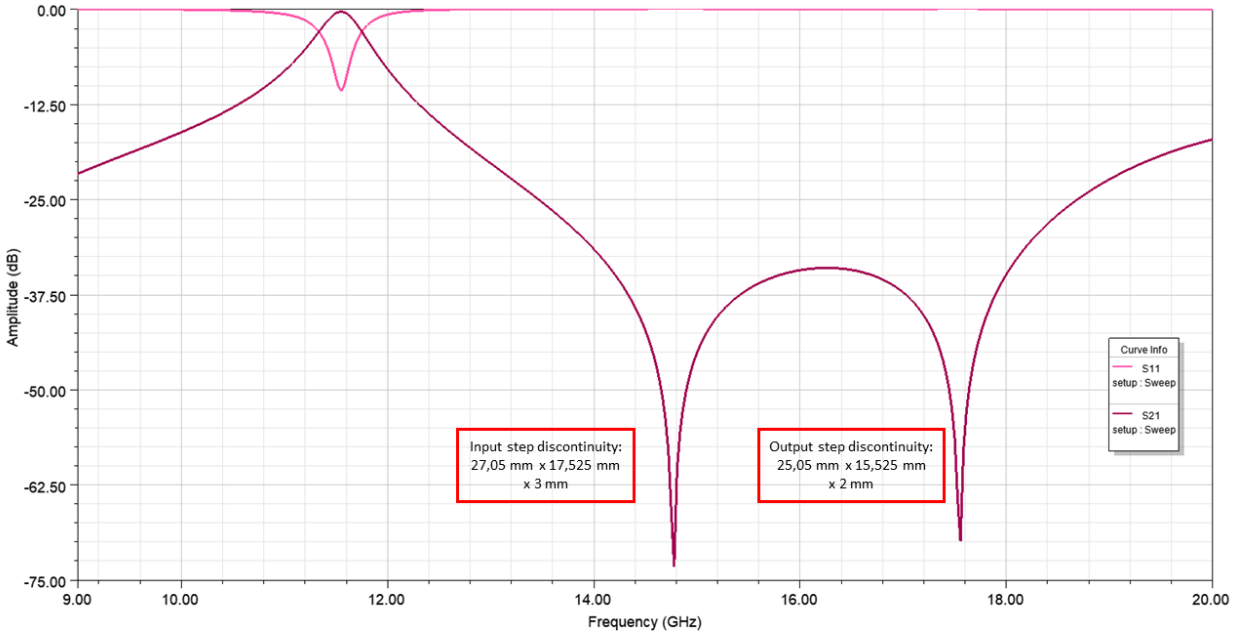

Figure 2.24: Resonant frequency of transmission zeros for the asymmetric filter in Fig. 2.23.

As we can observe, the transmission zero located closer to the passband corresponds to the bigger step discontinuity, while the one located at a higher frequency corresponds to the smaller step discontinuity. In this way, it is possible to control independently the frequency of these transmission zeros with the size of each step discontinuity.

Chapter 3

Filter design with FEST3D

3.1. Introduction

In this chapter we are going to study the process of filter design using the proposed technology, once it has been characterized in Chapter 2. We will start with the filter requirements and we will calculate from them the coupling matrix (M) [3]. Once the coupling matrix is obtained, we will calculate the external quality factor (Q_{ext}) and the inter-resonator couplings (k_{ij}). When we have these two parameters, using the tables and figures given in Chapter 2, we will obtain the physical dimensions of the filter, and we will simulate the resulting structure, that will be the starting point of the filter design. From here we will use the FEST3D [9] simulation and optimization tool to optimize the structure until it meets the initial requirements. Once we have the optimized filter, we will modify the structure in order to introduce transmission zeros to the design, as explained in Section 2.6.
In Table 3.1 we show the filters we are going to design applying the explained procedure. The initial requirements of these filters, such as their center frequency, return loss, bandwidth and fractional bandwidth (FBW) are given in Table 3.1.

Design	*Filter order*	*Center frequency* (GHz)	*Return loss* (dB)	*Bandwidth*	*FBW* (%)
1	3	11.5	22	500 MHz	4.34
2	3	11.5	22	1 GHz	8.69
3	3	11.5	22	2 GHz	17.39

Table 3.1: Requirements for the filters to be designed in this chapter.

We can observe than except from the 500 MHz bandwidth filter, the rest of the filters have big fractional bandwidths (FBW). This is because the technology allows very high couplings. In order to realize these filters, we have used the structure in Fig. 3.1.

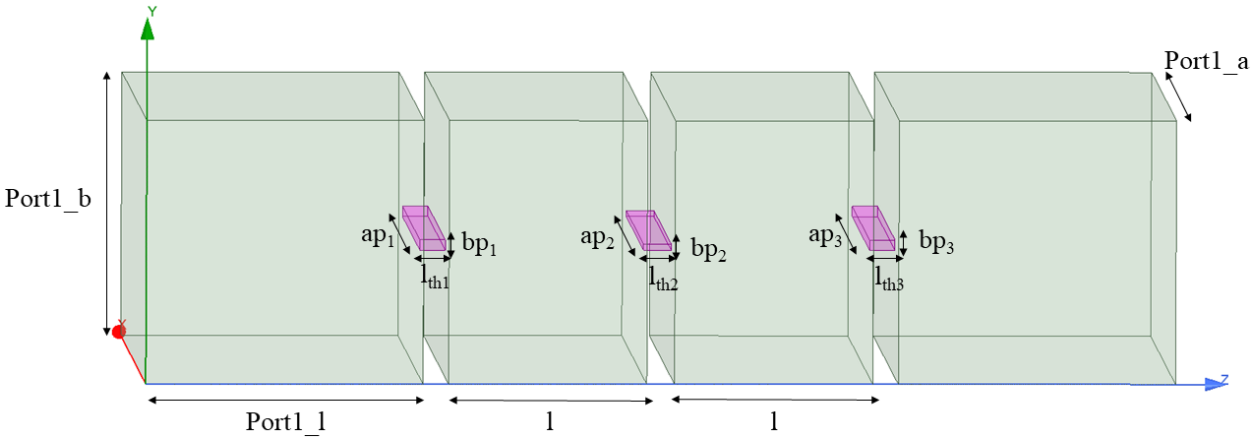

Figure 3.1: Generic structure of the third order filter under analysis.

3.2. Design of a 500 MHz bandwidth filter in Ku-band

As explained in the introduction, this first design consists of a third order filter with a center frequency of 11.5 GHz, a 500 MHz bandwidth (BW) and a return loss level of 22 dB (see Table 3.1).
Firstly, a MATLAB [10] routine has been implemented. This routine implements the inline filter synthesis explained in [3]. From the filter order and the return loss level given by the specifications, this routine calculates the g parameters. The g parameters are the circuital values of a low-pass filter normalized to port impedances of 1 Ω. From the g parameters, the routine calculates the coupling matrix (M). Once we have the coefficients of the coupling matrix (M), using the transformations explained in [3] we can obtain the inter-resonator couplings (k_{ij}) and the external quality factor (Q_{ext}). These transformations are the following:

$$k_{ij} = \frac{M_{ij}\, BW}{f_0} \tag{3.1}$$

$$Q_{ext} = \frac{f_0}{M_{S1}^2\, BW}, \tag{3.2}$$

where k_{ij} is the coupling coefficient between resonators i and j, M_{ij} is the normalized inter-resonator coupling between the resonators i and j, M_{S1} is the normalized coupling between the source and the first resonator, BW is the bandwidth of the filter, f_0 is the center frequency of the filter and Q_{ext} is the computed external quality factor. For the three designs of this chapter, the coupling matrix is the following:

$$M = \begin{pmatrix} 0 & 1.1375 & 0 & 0 & 0 \\ 1.1375 & 0 & 1.1010 & 0 & 0 \\ 0 & 1.1010 & 0 & 1.1010 & 0 \\ 0 & 0 & 1.1010 & 0 & 1.1375 \\ 0 & 0 & 0 & 1.1375 & 0 \end{pmatrix} \tag{3.3}$$

It should be noted that for third order filters there is only one different inter-resonator coupling (k_{ij}). Therefore, we go from the coefficients of the coupling matrix (M) to the parameters that characterize the filter:

$$\begin{cases} M_{S1} = 1.1375 \\ M_{ij} = 1.1010 \end{cases} \longrightarrow \begin{cases} Q_{ext} = 17.77 \\ k_{ij} = 0.0479 \end{cases}$$

Now we are ready to use the figures and tables in Chapter 2 in order to obtain the initial physical dimensions of the filter. If we look at Fig. 3.2, we can obtain, from the Q_{ext} values calculated in Chapter 2, the closest value to the one we need for the starting point of the filter. This could also have been addressed by solving an interpolation problem in order to obtain the exact value of Q_{ext}, but for simplicity and since after this starting point we will perform an optimization process, this approximation has been chosen.

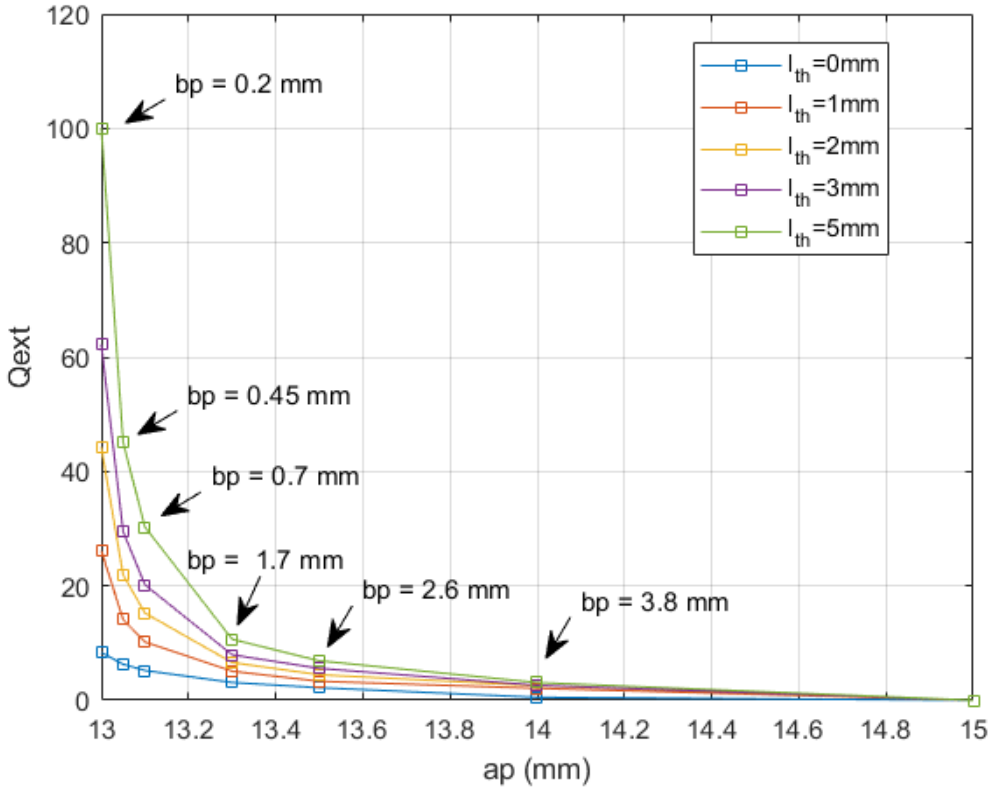

Figure 3.2: Variation of the Q_{ext} as a function of ap, for different l_{th}.

We can see that with a 13.05 mm × 0.45 mm × 2 mm aperture we obtain a Q_{ext}= 21.92.
Now we look at the inter-resonator coupling (k) figure for a 13.05 mm × 0.45 mm aperture and looking at the curve for l_{th}= 2 mm, we obtain the length of the intermediate waveguide section (l) that we need to get the closest value to the desired k. In Fig. 3.3 we observe that with l= 7 mm we have a k=0.0479.

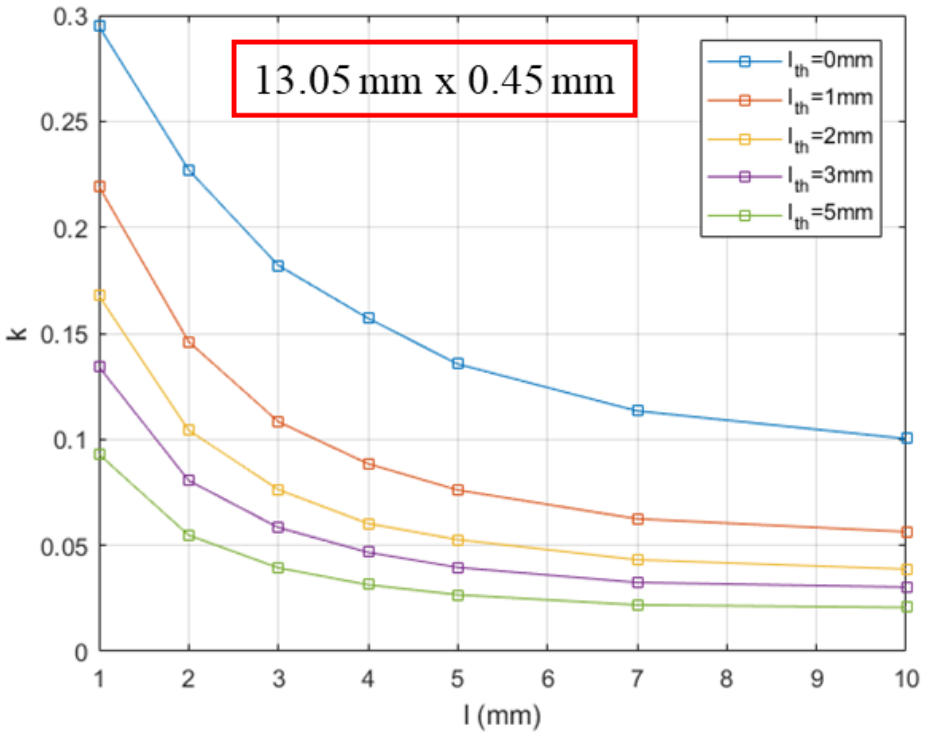

Figure 3.3: Inter-resonator coupling as a function of l (mm), for different l_{th} (mm), for a 13.05 mm $\times$ 0.45 mm resonant iris.

The initial physical dimensions for this filter are collected in Table 3.2.

Variable	*Value* (mm)
$Port1a$	19.05
$Port1b$	9.525
$Port1l$	10
$ap_1 = ap_3$	13.05
$bp_1 = bp_3$	0.45
$l_{th_1} = l_{th3}$	2
l	7
ap_2	13.05
bp_2	0.45
l_{th2}	2

Table 3.2: Initial dimensions for the 500 MHz bandwidth filter, according to the schematic shown in Fig. 3.1.

Now we can simulate this first aproximation of the filter and obtain the starting point of the design, shown in Fig. 3.4.

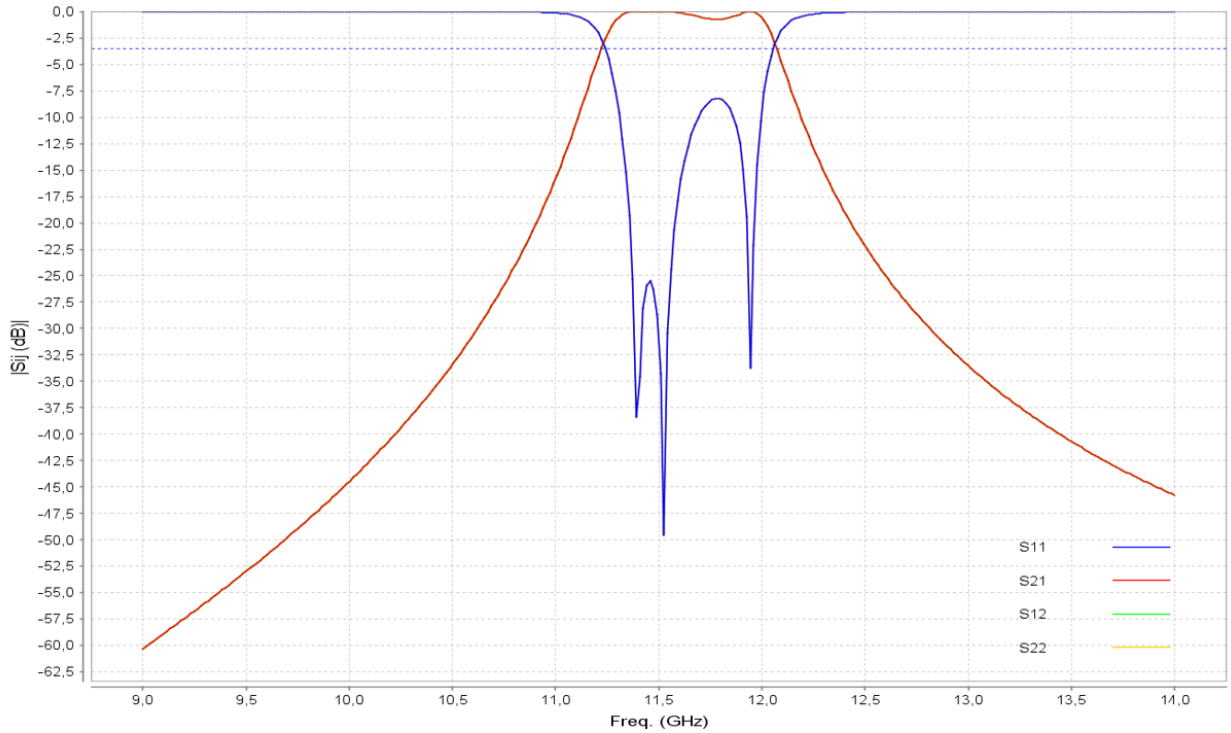

Figure 3.4: S parameters response of the initial point for the 500 MHz bandwidth filter.

We can observe that, in this case, we have obtained a center frequency of 11.52 GHz, a bandwidth of 550 MHz and the return loss level is 8.74 dB. The first thing we do to optimize this design is to adjust the center frequency to 11.5 GHz, by slightly modifying the width and the height of the aperture (as we have studied in Chapter 2). Then we increase the length of the intermediate waveguide section (l). In this way, the inter-resonator coupling (k) decreases, and this leads to a decrement in the bandwidth and an improvement in the return losses. When we do this, normally we need to readjust some variables to tune the filter response and to obtain the right return losses. Using the FEST3D optimizer, we will modify the filter response until it meets the initial requirements. The optimized response is shown in Fig. 3.5.

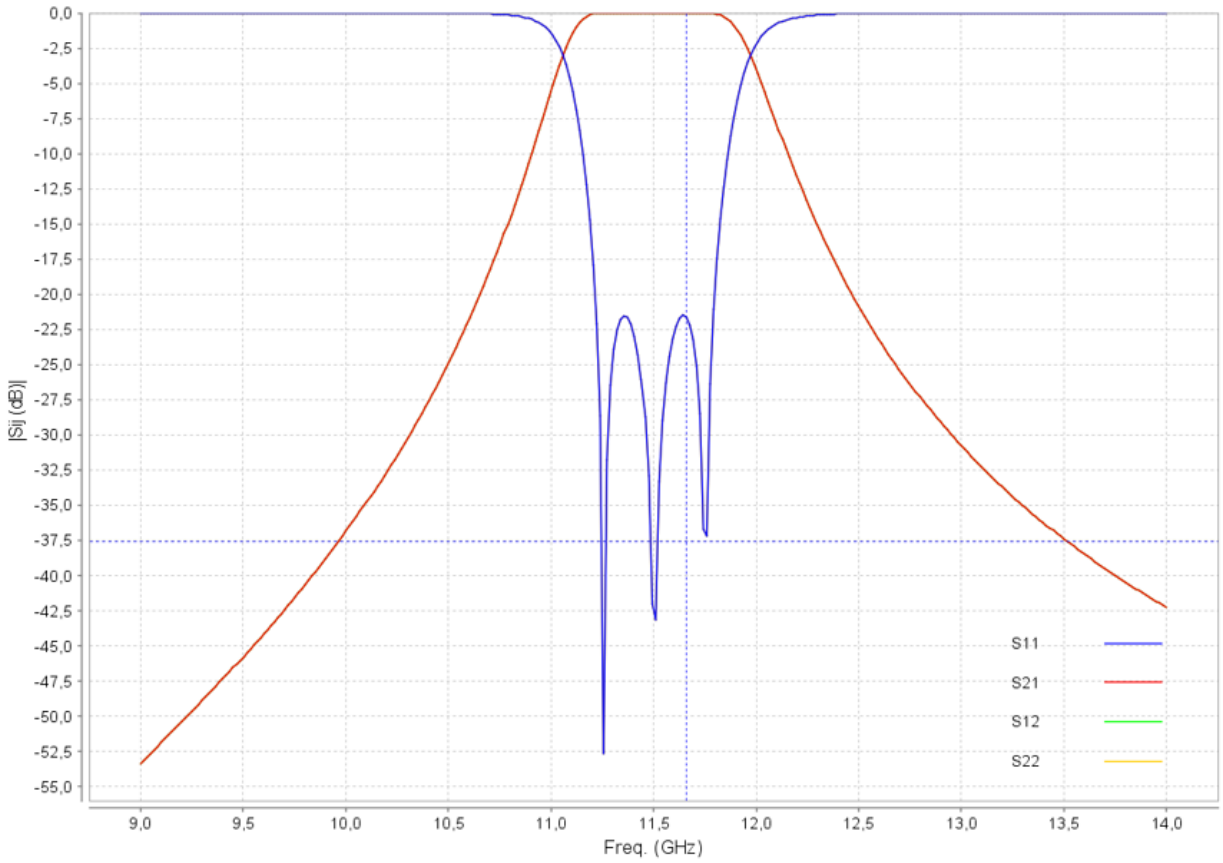

Figure 3.5: S parameters response of the optimized 500 MHz bandwidth filter.

Therefore we have the final dimensions for the filter. These dimensions are reported in Table 3.3. It should be noted that there is not a single solution for these filter requirements. Other dimensions could lead to this same filter response.

Variable	*Value* (mm)
$Port1a$	19.05
$Port1b$	9.525
$Port1l$	10
$ap_1 = ap_3$	13.19
$bp_1 = bp_3$	0.37
$l_{th_1} = l_{th3}$	0.92
l	7.15
ap_2	13.22
bp_2	0.22
l_{th2}	1

Table 3.3: Final dimensions for the 500 MHz bandwidth filter.

In Table 3.4 we show the comparative between the initial and the final dimensions of the filter.

Variable	*Initial value* (mm)	*Final value* (mm)	*Relative error*
$Port1a$	19.05	19.05	-
$Port1b$	9.525	9.525	-
$Port1l$	10	10	-
$ap_1 = ap_3$	13.05	13.19	0.01
$bp_1 = bp_3$	0.45	0.37	-0.22
$l_{th_1} = l_{th3}$	2	0.92	-1.17
l	7	7.15	0.02
ap_2	13.05	13.22	0.01
bp_2	0.45	0.22	-1.04
l_{th2}	2	1	-1

Table 3.4: Comparative between the initial and final dimensions for the 500 MHz bandwidth filter.

In this case the optimized geometry can be seen in Fig. 3.6.

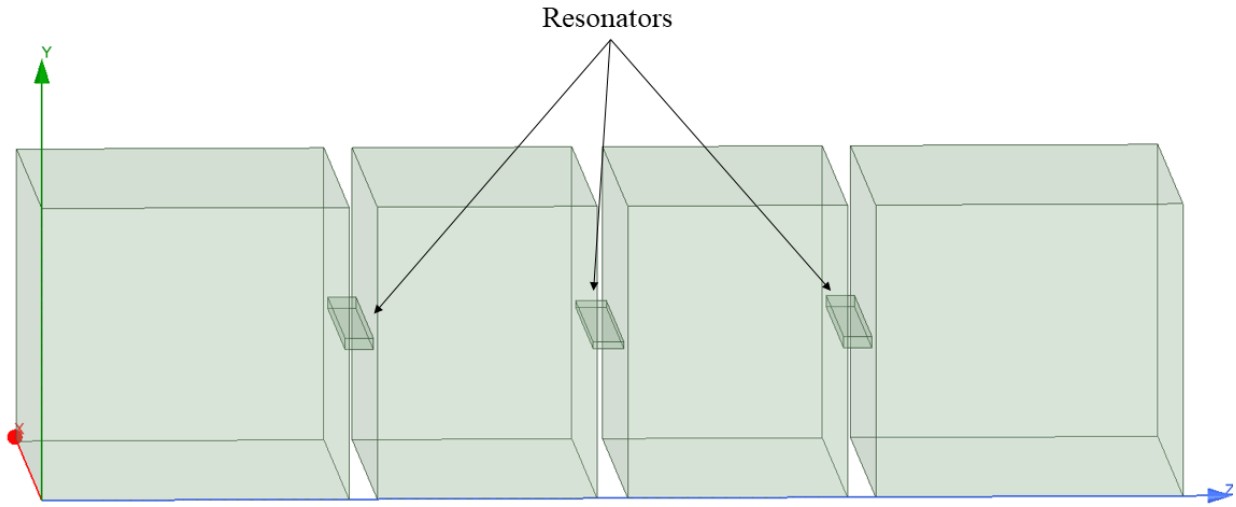

Figure 3.6: Optimized geometry for the 500 MHz bandwidth filter.

The total physical dimensions for this filter are 19.05 mm × 9.525 mm × 37.14 mm. If we transform these physical dimmensions to the electrical dimensions by dividing by $\lambda = \frac{c}{f_0} = 0.0261$, we obtain a filter of 0.73 × 0.365 × 1.423.

$$\left\{ \begin{array}{l} \text{Physical dimensions:} \\ 19.05 \text{ mm} \times 9.525 \text{ mm} \times 37.14 \text{ mm} \end{array} \right. \longrightarrow \left\{ \begin{array}{l} \text{Electrical dimensions:} \\ 0.73 \times 0.365 \times 1.423 \end{array} \right.$$

Now that we have our optimized filter, we are going to introduce transmission zeros to the design. For this, we add a step discontinuity between the source and the first resonator and between the last resonator and the load, as shown in Fig. 3.7.

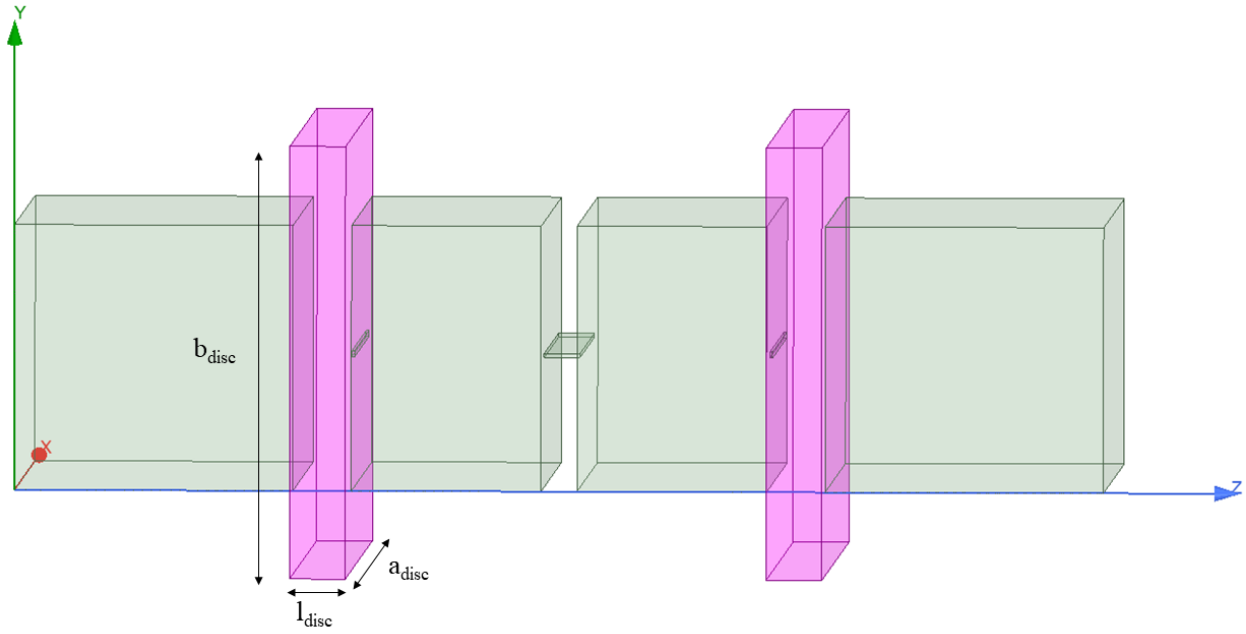

Figure 3.7: Optimized geometry for the 500 MHz bandwidth filter with two step discontinuities.

In order to introduce these transmission zeros, it is important to bring them closer to the passband slowly. Besides, when we introduce them to the design, the return losses usually get worse, and therefore we need to modify a little bit some of the variables so that the filter meets the requirements. In Chapter 2 we have studied that the bigger the dimensions of the step discontinuities are, the lower the frequency of the transmission zeros is. That is why in this case we have started with two step discontinuities which dimensions ($a_{disc} \times b_{disc} \times l_{disc}$) are 25.05 mm $\times$ 15.525 mm $\times$ 2 mm. After an optimization process using the FEST3D optimization tool, we obtain the frequency response shown in Fig. 3.8.

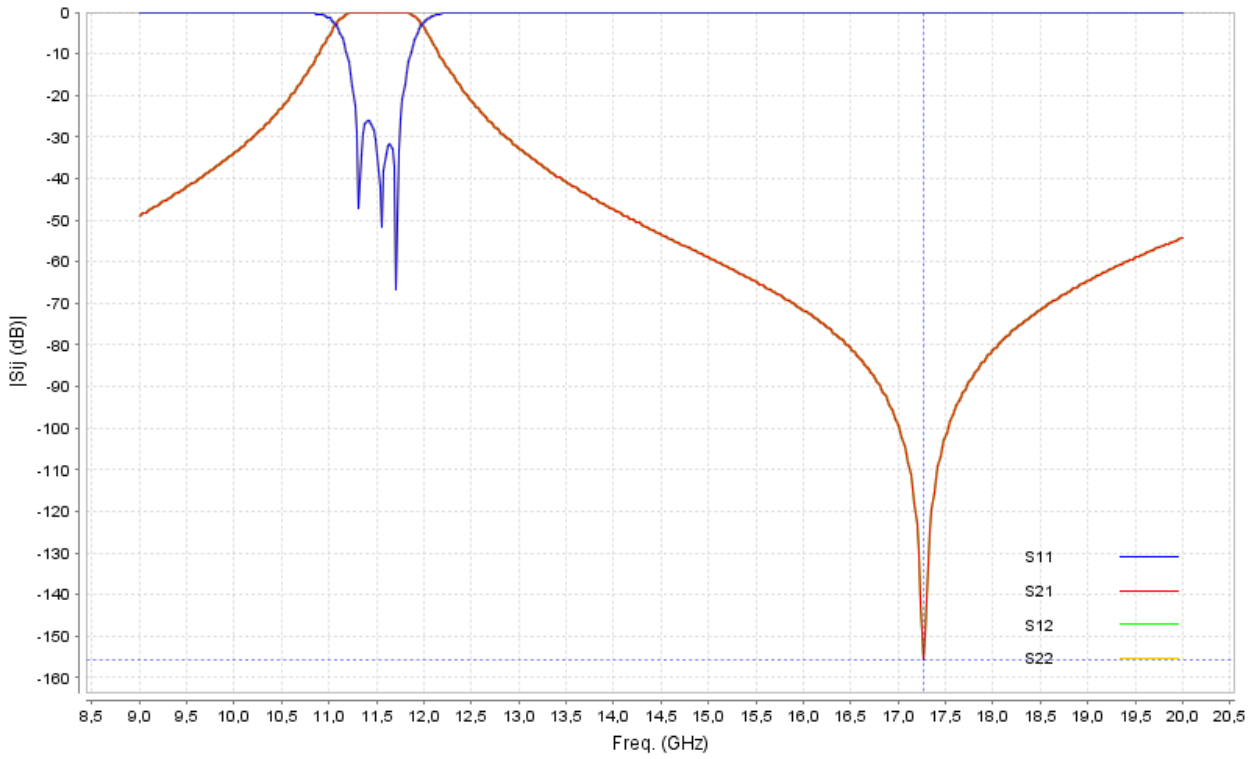

Figure 3.8: S parameters response of the 500 MHz bandwidth filter when adding two 25.05 mm × 15.525 mm × 2 mm step discontinuities.

In Table 3.5 we can see the final dimensions of the filter when we add these step discontinuities.

Variable	*Value* (mm)
$Port1a$	19.05
$Port1b$	9.525
$Port1l$	10
$ap_1 = ap_3$	13.41
$bp_1 = bp_3$	0.21
$l_{th_1} = l_{th3}$	0.1
l	6.81
ap_2	13.16
bp_2	0.14
l_{th2}	1.29
a_{disc}	25.05
b_{disc}	15.525
l_{disc}	2

Table 3.5: Final dimensions for the 500 MHz bandwidth filter when adding two 25.05 mm × 15.525 mm × 2 mm step discontinuities.

Now we are going to bring the transmission zeros closer. For this, the dimensions of the step discontinuities ($a_{disc} \times b_{disc} \times l_{disc}$) will be in this case 26.05 mm × 16.525 mm × 2 mm. Once we introduce the discontinuities, we tune the filter as it has been explained. We can see the final frequency response in Fig. 3.9 and the dimensions for this case in Table 3.6.

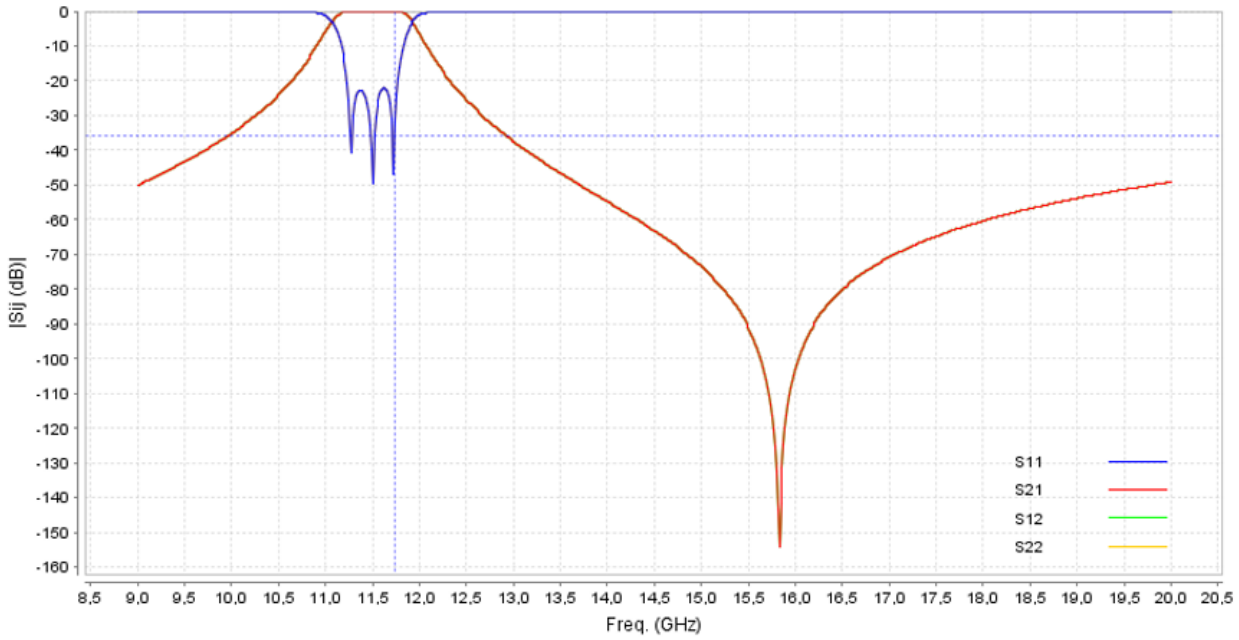

Figure 3.9: S parameters response of the 500 MHz bandwidth filter when adding two 26.05 mm × 16.525 mm × 2 mm step discontinuities.

Variable	*Value* (mm)
$Port1a$	19.05
$Port1b$	9.525
$Port1l$	10
$ap_1 = ap_3$	13.46
$bp_1 = bp_3$	0.21
$l_{th_1} = l_{th3}$	0.1
l	6.78
ap_2	13.18
bp_2	0.14
l_{th2}	1.57
a_{disc}	26.05
b_{disc}	16.525
l_{disc}	2

Table 3.6: Final dimensions for the 500 MHz bandwidth filter when adding two 26.05 mm × 16.525 mm × 2 mm step discontinuities.

If we wanted to bring the transmission zeros closer to the passband, we could apply this procedure again. The total physical dimensions of the filter, shown in Fig. 3.7, are 26.05 mm × 16.525 mm × 39.33 mm, and by dividing by $\lambda = \frac{c}{f_0} = 0.0261$, we obtain a filter of electric dimensions 0.998 × 0.615 × 1.51.

$$\begin{cases} \text{Physical dimensions:} \\ 26.05 \text{ mm} \times 16.525 \text{ mm} \times 37.14 \text{ mm} \end{cases} \longrightarrow \begin{cases} \text{Electrical dimensions:} \\ 0.998 \times 0.615 \times 1.51 \end{cases}$$

3.3. Design of a 1 GHz bandwidth filter in Ku-band

Now we are going to design a filter with a center frequency of 11.5 GHz, a 1 GHz bandwidth and a return loss level of 22 dB.
The first step, as we already know, is to go from the coefficients of the coupling matrix (M) to the parameters that characterize the filter, using equations (3.1) and (3.2). The coupling matrix is the same as the one used in the previous study, and is shown in equation (3.3). Therefore we have:

$$\begin{cases} M_{S1} = 1.1375 \\ M_{ij} = 1.1010 \end{cases} \longrightarrow \begin{cases} Q_{ext} = 8.8 \\ k_{ij} = 0.0957 \end{cases}$$

Now we are going to obtain the physical dimensions of the filter. Using Fig. 3.10 we obtain the dimensions of the apertures in order to get the Q_{ext} vlaue as close as possible to the desired one.

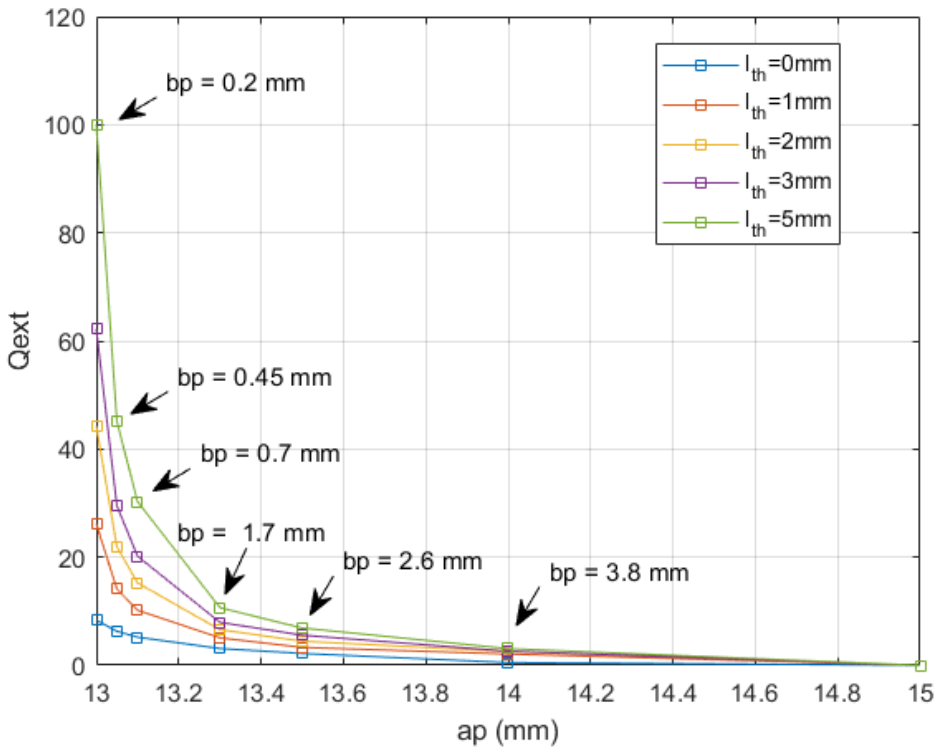

Figure 3.10: Variation of the Q_{ext} as a function of ap, for different l_{th}.

We can see that with a 13 mm × 0.2 mm × 0.01 mm aperture we obtain a Q_{ext}= 8.3.
Now we look at Fig. 3.11, where we see the inter-resonator coupling (k) for a 13 mm × 0.2 mm aperture. From this figure, looking at the curve for l_{th} = 0 mm, we obtain the length of the intermediate waveguide section (l) that we need to get the closest value to the wanted k. In this case we need l= 7 mm in order to get a k=0.094.

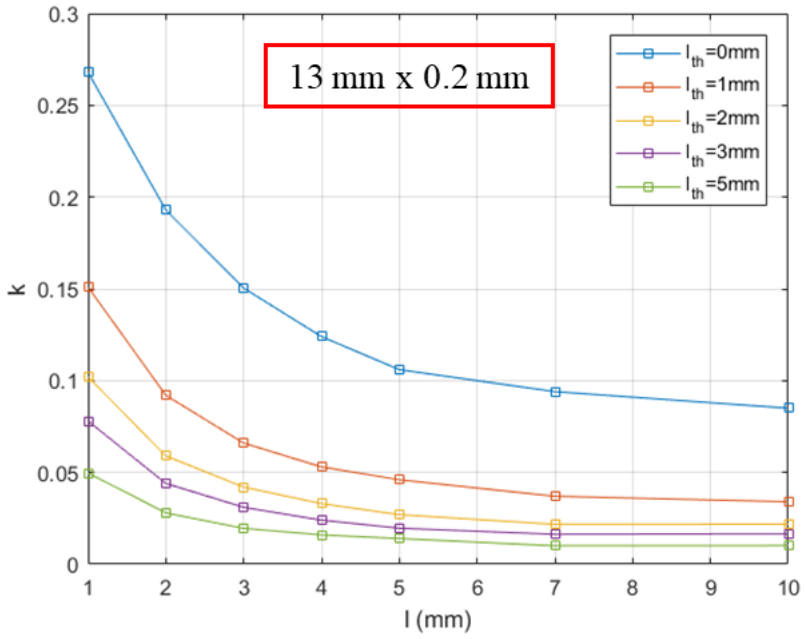

Figure 3.11: Inter-resonator coupling as a function of l (mm), for different l_{th} (mm), for a 13 mm × 0.2 mm iris.

The initial physical dimensions for this design are shown in Table 3.7.

Variable	*Value* (mm)
$Port1a$	19.05
$Port1b$	9.525
$Port1l$	10
$ap_1 = ap_3$	13
$bp_1 = bp_3$	0.2
$l_{th_1} = l_{th3}$	0.01
l	7
ap_2	13
bp_2	0.2
l_{th2}	0.01

Table 3.7: Initial dimensions for the 1 GHz bandwidth filter.

Now we simulate this first aproximation of the filter and obtain the starting point of the design, which is shown in Fig. 3.12.

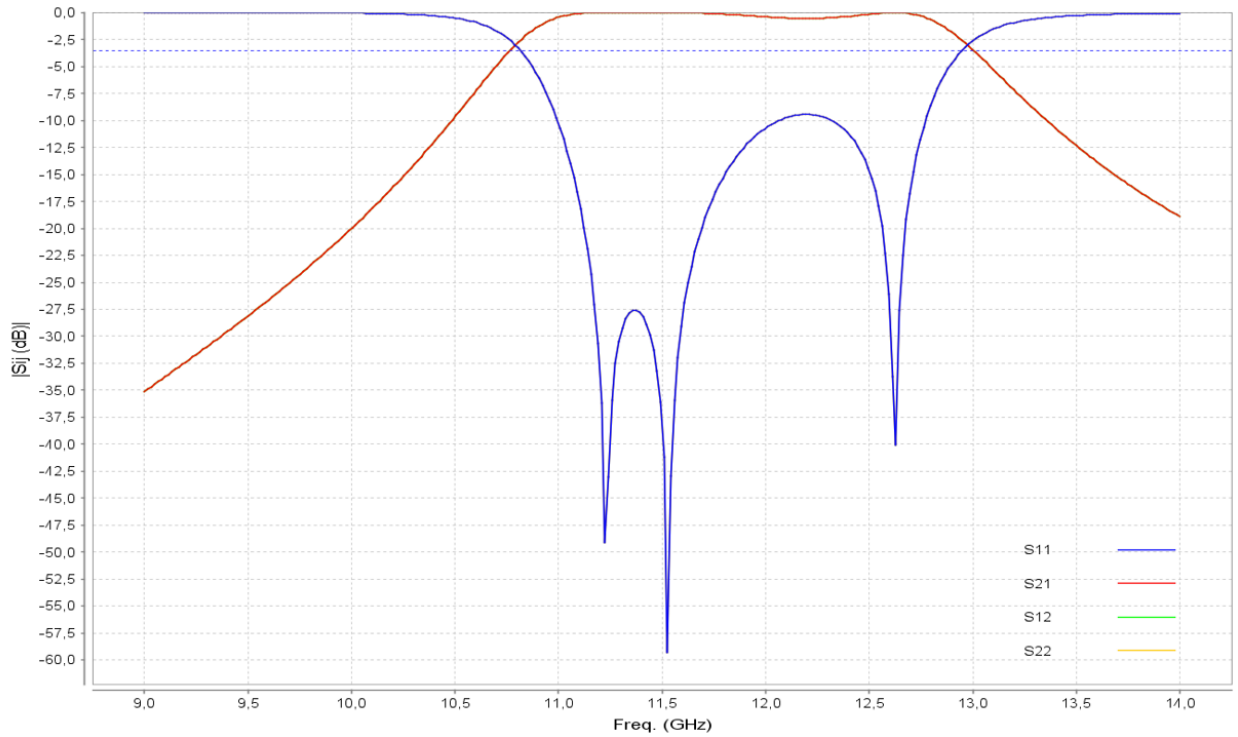

Figure 3.12: S parameters response of the first aproximation for the 1 GHz bandwidth filter.

In this first aproximation, we have obtained a center frequency of 11.525 GHz, a bandwidth of 1.4 GHz and a return loss level of 9.43 dB. As we have done in the previous design, we move the center frequency of the filter to the desired one, we equalize the filter, and using the FEST3D optimization tool, we optimize the filter response until we obtain a bandwidth of 1 GHz, a center frequency of 11.5 GHz and until the return losses are 22 dB. As we have explained in the previous design, there are several filter dimensions that lead to the same filter response. For example, in this case, we have obtained two different valid solutions for the optimization. In Fig. 3.13 we see the frequency response of the first solution for the optimization.

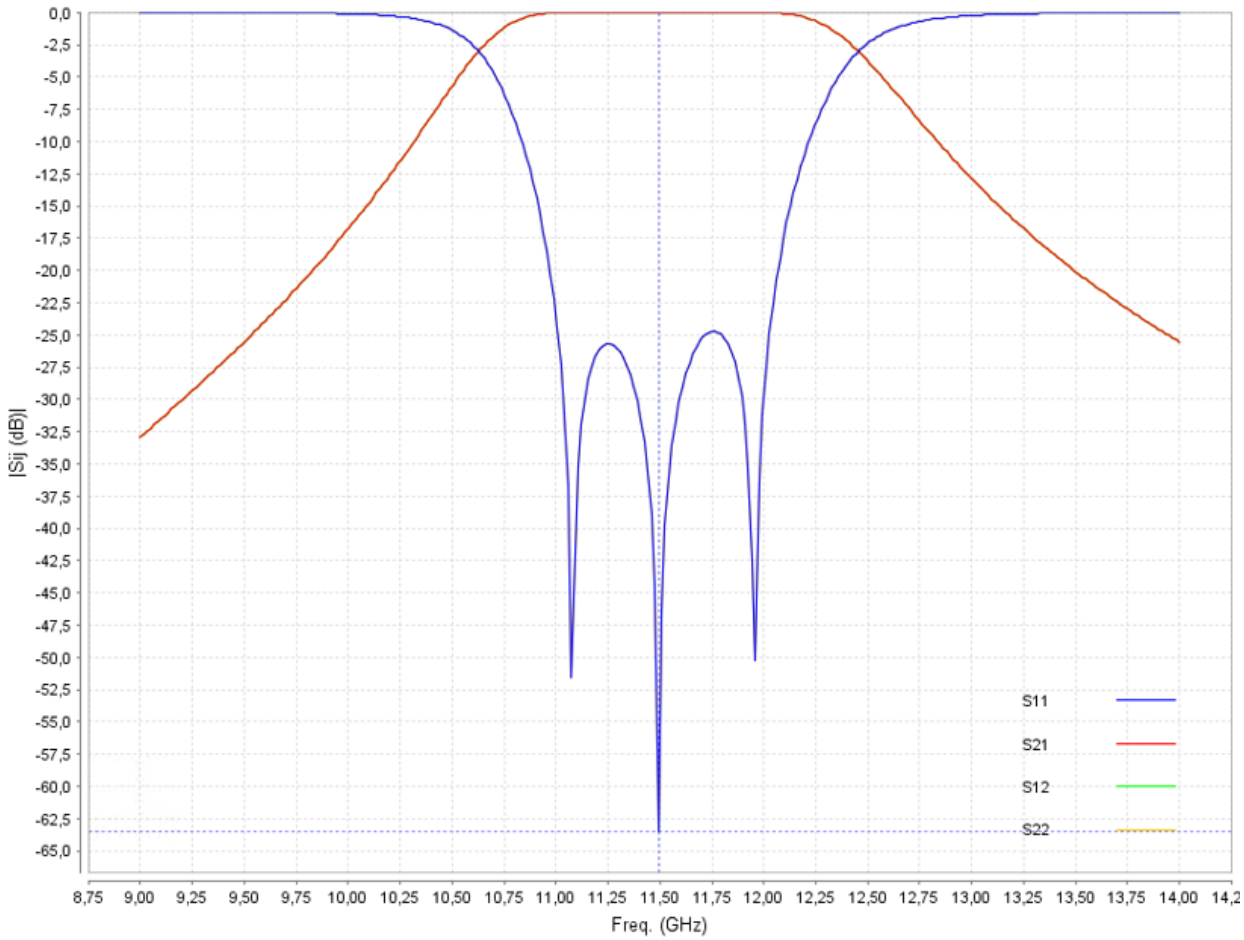

Figure 3.13: S parameters response of the first optimization for the 1 GHz bandwidth filter.

In Table 3.8 we can see the final dimensions for this first optimization.

Variable	*Value* (mm)
$Port1a$	19.05
$Port1b$	9.525
$Port1l$	10
$ap_1 = ap_3$	14.92
$bp_1 = bp_3$	0.36
$l_{th_1} = l_{th3}$	0.2
l	2.6
ap_2	13.43
bp_2	0.35
l_{th2}	5.98

Table 3.8: Final dimensions of the first optimization for the 1 GHz bandwidth filter.

The optimized geometry for this solution can be seen in Fig. 3.14. The total physical dimensions of the filter are 19.05 mm × 9.525 mm × 31.58 mm, and the electrical dimensions of the filter, calculated by dividing by $\lambda = \frac{c}{f_0} = 0.0261$, are 0.73 × 0.365 × 1.21.

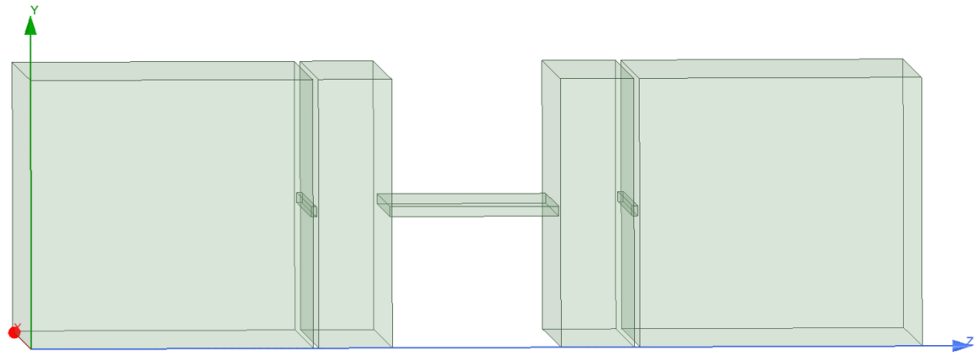

Figure 3.14: First optimized geometry for the 1 GHz bandwidth filter.

$$\begin{cases} \text{Physical dimensions:} \\ 19.05 \text{ mm} \times 9.525 \text{ mm} \times 31.58 \text{ mm} \end{cases} \longrightarrow \begin{cases} \text{Electrical dimensions:} \\ 0.73 \times 0.365 \times 1.21 \end{cases}$$

This filter meets the specifications, but we have tried to get to a different solution where the central resonator is shorter. In Fig. 3.15 we can see the frequency response of the second optimized design where the central resonator is shorter than in the previous one.

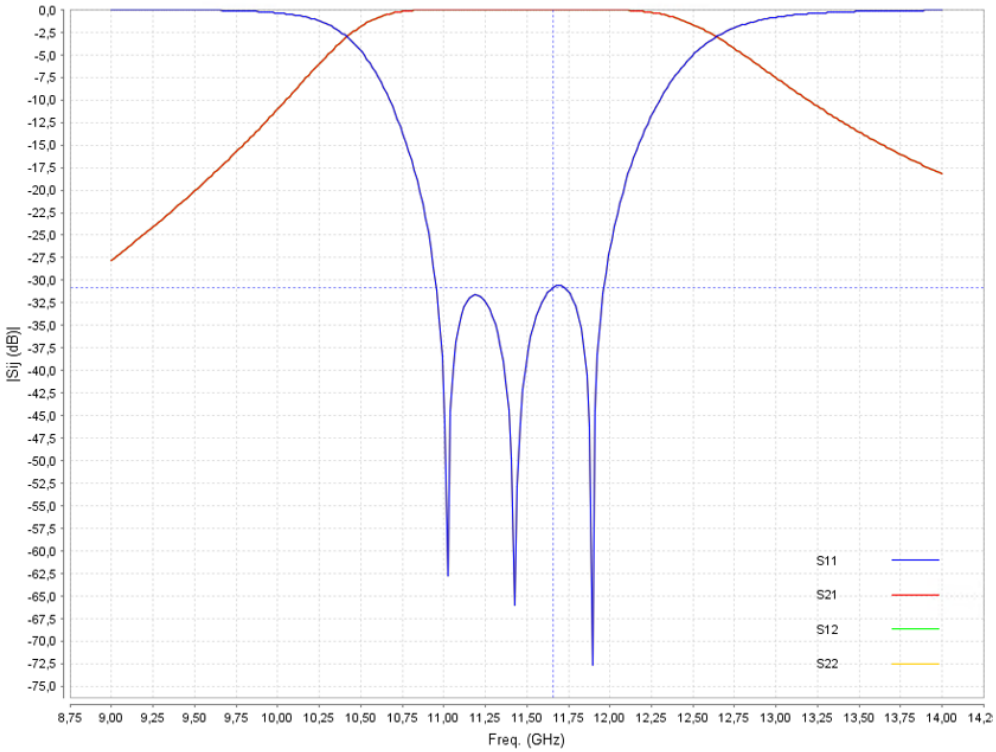

Figure 3.15: S parameters response of the second optimization for the 1 GHz bandwidth filter.

The final dimensions of the second optimization for this filter can be seen in Table 3.9.

Variable	*Value* (mm)
$Port1a$	19.05
$Port1b$	9.525
$Port1l$	10
$ap_1 = ap_3$	13.5
$bp_1 = bp_3$	1.14
$l_{th_1} = l_{th3}$	0.3
l	7.6
ap_2	13.41
bp_2	0.22
l_{th2}	0.1

Table 3.9: Final dimensions of the second optimization for the 1 GHz bandwidth filter.

The optimized geometry for this solution is shown in Fig. 3.16. The total physical dimensions of the filter are 19.05 mm × 9.525 mm × 35.9 mm, and the electrical dimensions of the filter, calculated by dividing by $\lambda = \frac{c}{f_0} = 0.0261$, are 0.73 × 0.365 × 1.376.

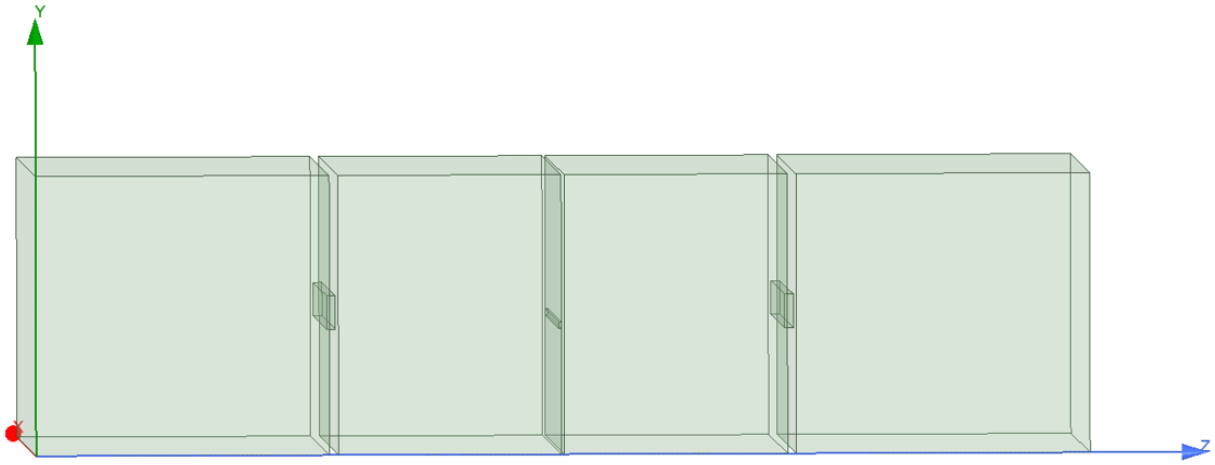

Figure 3.16: Final optimized geometry of the 1 GHz bandwidth filter.

$$\left\{ \begin{array}{l} \text{Physical dimensions:} \\ 19.05 \text{ mm} \times 9.525 \text{ mm} \times 35.9 \text{ mm} \end{array} \right. \longrightarrow \left\{ \begin{array}{l} \text{Electrical dimensions:} \\ 0.73 \times 0.365 \times 1.376 \end{array} \right.$$

Now we are going to compare these two optimizations. In Fig. 3.17 we can see the frequency response of the two optimizations.

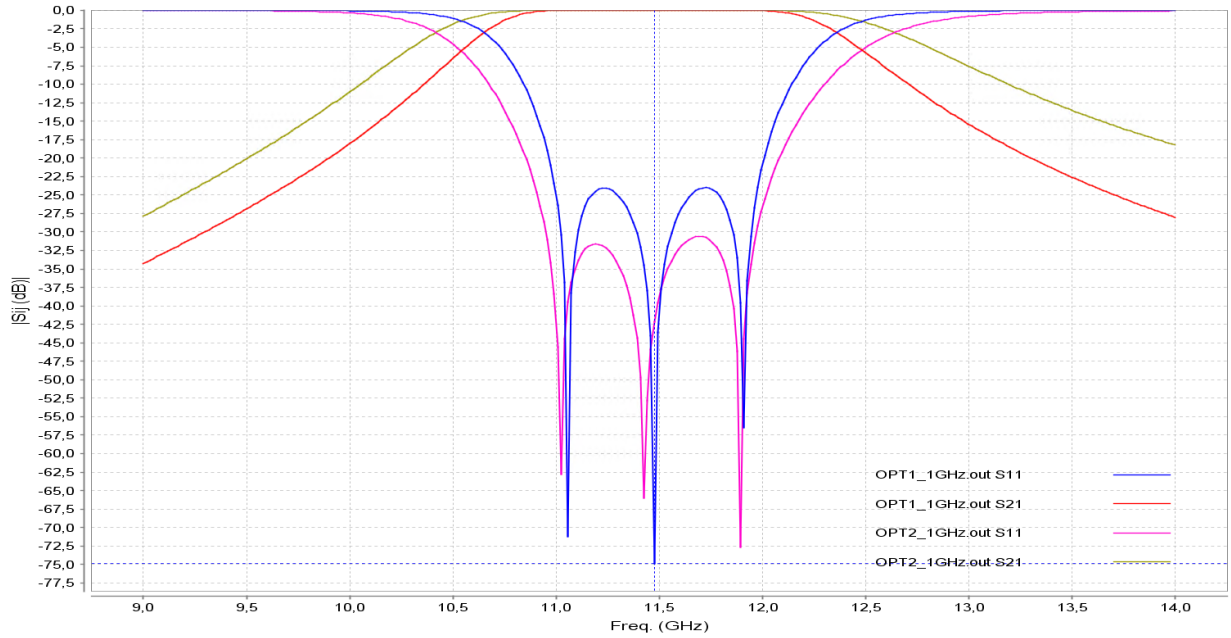

Figure 3.17: S parameter comparison of the two optimizations for the 1 GHz bandwidth filter.

We can observe, that even though the two optimizations meet the initial requirements, there are some differences between the two frequency responses. On the one hand, the first optimization (OPT_1) has a lower return loss level than the second optimization (OPT_2). However, the S_{21} parameter of the first optimization, (OPT_1) decreases more quickly than the S_{21} parameter of the second optimization (OPT_2). In Table 3.10 we show the comparative between the initial and the final dimensions of the filter for the first optimization (OPT_1) and the second optimization (OPT_2).

		OPT_1		OPT_2	
Variable	*Initial value* (mm)	*Final value* (mm)	*Relative error*	*Final value* (mm)	*Relative error*
$Port1a$	19.05	19.05	-	19.05	-
$Port1b$	9.525	9.525	-	9.525	-
$Port1l$	10	10	-	10	-
$ap_1 = ap_3$	13	14.92	0.13	13.5	0.04
$bp_1 = bp_3$	0.2	0.36	0.44	1.14	0.82
$l_{th_1} = l_{th3}$	0.01	0.2	0.95	0.3	0.97
l	7	2.6	-1.69	7.6	0.08
ap_2	13	13.43	0.03	13.41	0.03
bp_2	0.2	0.35	0.43	0.22	0.09
l_{th_2}	0.01	5.98	0.99	0.1	0.9

Table 3.10: Comparative between the dimensions of the 1 GHz bandwidth filter for the two optimizations.

We can see that in the first optimization (OPT_1), the strategy is to reduce the inter-resonator coupling (k) by increasing the thickness of the central resonant aperture l_{th_2}, while in the second solution, the reduction of the inter-resonator coupling (k) is achieved by reducing the width and height of the central resonator

($ap_2 \times bp_2$). This will therefore affect the unloaded quality factor (Q_u), since bigger resonators have higher Q_u. Finally, in Table 3.11 we can see a comparison between the final size of the 1 GHz bandwidth filter for the two optimizations.

Design	*Physical dimensions (mm)*	*Electrical dimensions*
OPT_1	$19.05 \times 9.525 \times 31.58$	$0.73 \times 0.365 \times 1.21$
OPT_2	$19.05 \times 9.525 \times 35.9$	$0.73 \times 0.365 \times 1.376$

Table 3.11: Final size comparison between the two optimizations for the 1 GHz bandwidth filter.

We can see that the first optimization (OPT_1) leads to a shorter filter than the second optimization (OPT_2). We can conclude that depending on the aditional restrictions that we may have in the design process, such as out of band requirements, unloaded quality factor (Q_u) or size restrictions, we will be able to choose between the two optimizations.

3.4. Design of a 2 GHz bandwidth filter in Ku-band

To end this chapter, we are going to design a third order filter with a center frequency of 11.5 GHz, a 2 GHz bandwidth and a return loss level of 22 dB. Using equations (3.1) and (3.2) we calculate the external quality factor (Q_{ext}) and the inter-resonator coupling (k) from the coupling matrix (M), shown in equation (3.3). Therefore, we have:

$$\begin{cases} M_{S1} = 1.1375 \\ M_{ij} = 1.1010 \end{cases} \longrightarrow \begin{cases} Q_{ext} = 4.4 \\ k_{ij} = 0.1915 \end{cases}$$

We can see that when we have to design a filter with higher bandwidth, we need a lower Q_{ext} and a higher k. Now we need to go from this parameters to the physical dimensions of the filter, and for that we will use the figures of Chapter 2. If we look at Fig. 3.18 we will obtain the width, height and thickness of the aperture in order to get the closest value to the Q_{ext} we are looking for.

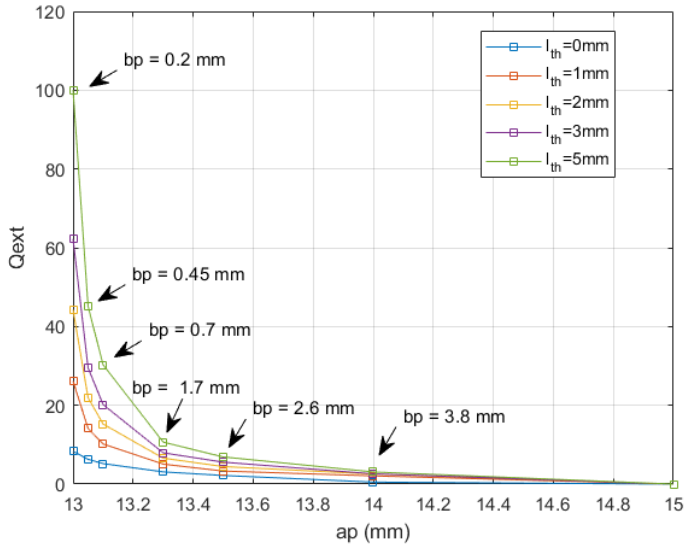

Figure 3.18: Variation of the Q_{ext} as a function of ap, for different l_{th}.

We observe that with a 13.5 mm × 2.6 mm × 2 mm aperture we get a Q_{ext}= 4.45. With this, we look at the figure of the inter-resonator coupling as a function of the length of the intermediate waveguide section (l) for a 13.5 mm × 2.6 mm aperture. As we can see in Fig. 3.19, looking at the curve for l_{th} = 2 mm, if l= 3 mm, then k=0.198.

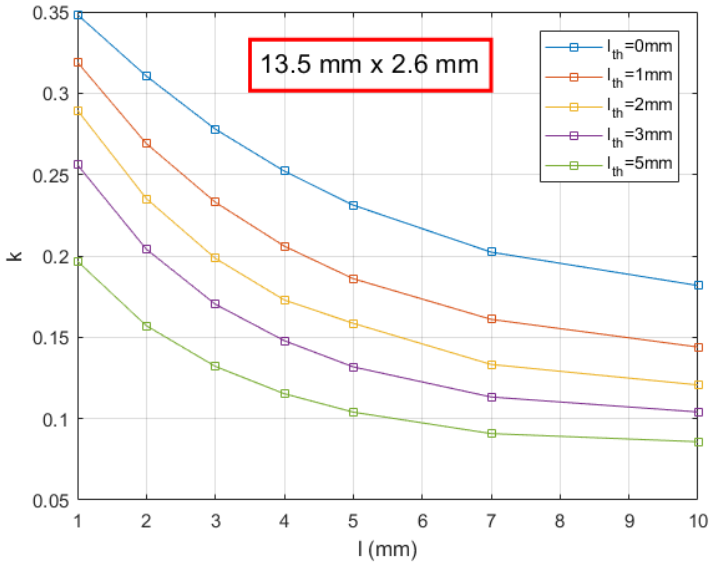

Figure 3.19: Inter-resonator coupling as a function of l (mm), for different l_{th} (mm), for a 13.5 mm × 2.6 mm iris.

Therefore, the initial physical dimensions for this design are:

Variable	*Value* (mm)
$Port1a$	19.05
$Port1b$	9.525
$Port1l$	10
$ap_1 = ap_3$	13.5
$bp_1 = bp_3$	2.6
$l_{th_1} = l_{th3}$	2
l	3
ap_2	13.5
bp_2	2.6
l_{th2}	2

Table 3.12: Initial dimensions for the 2 GHz bandwidth filter.

From here, we simulate the first aproximation of the filter. The starting point of the design is shown in Fig. 3.20.

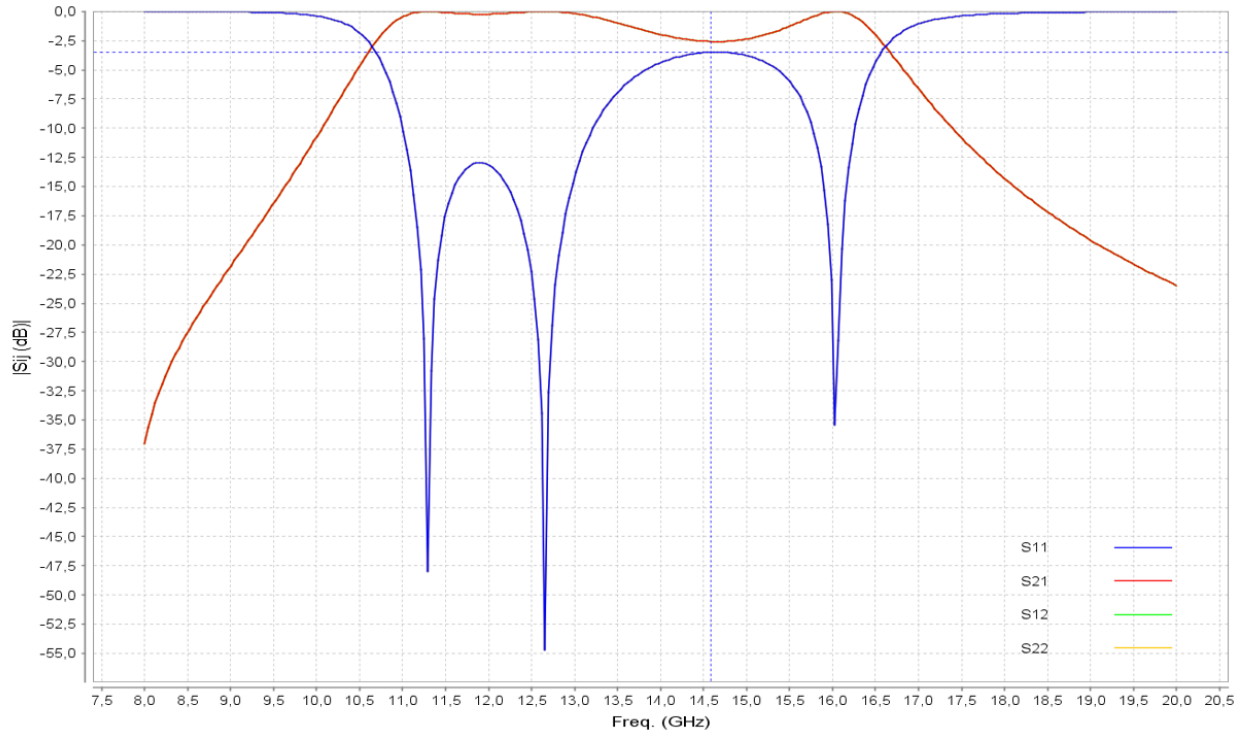

Figure 3.20: S parameters reponse of the first aproximation for the 2 GHz bandwidth filter.

In this case we can see that we have obtained a center frequency of 12.65 GHz, a bandwidth of 4.73 GHz and a return loss level of 3.49 dB. As we can observe, as we increase the bandwidth of the designed filter, the starting point get worse. This is due to the narrow band approximation assumed in the coupling matrix formalism. However, although at first it can be a little bit difficult to center the filter in 11.5 GHz, once we do that the filter is optimized easily using the FEST3D optimization tool. The optimized design is shown in Fig. 3.21.

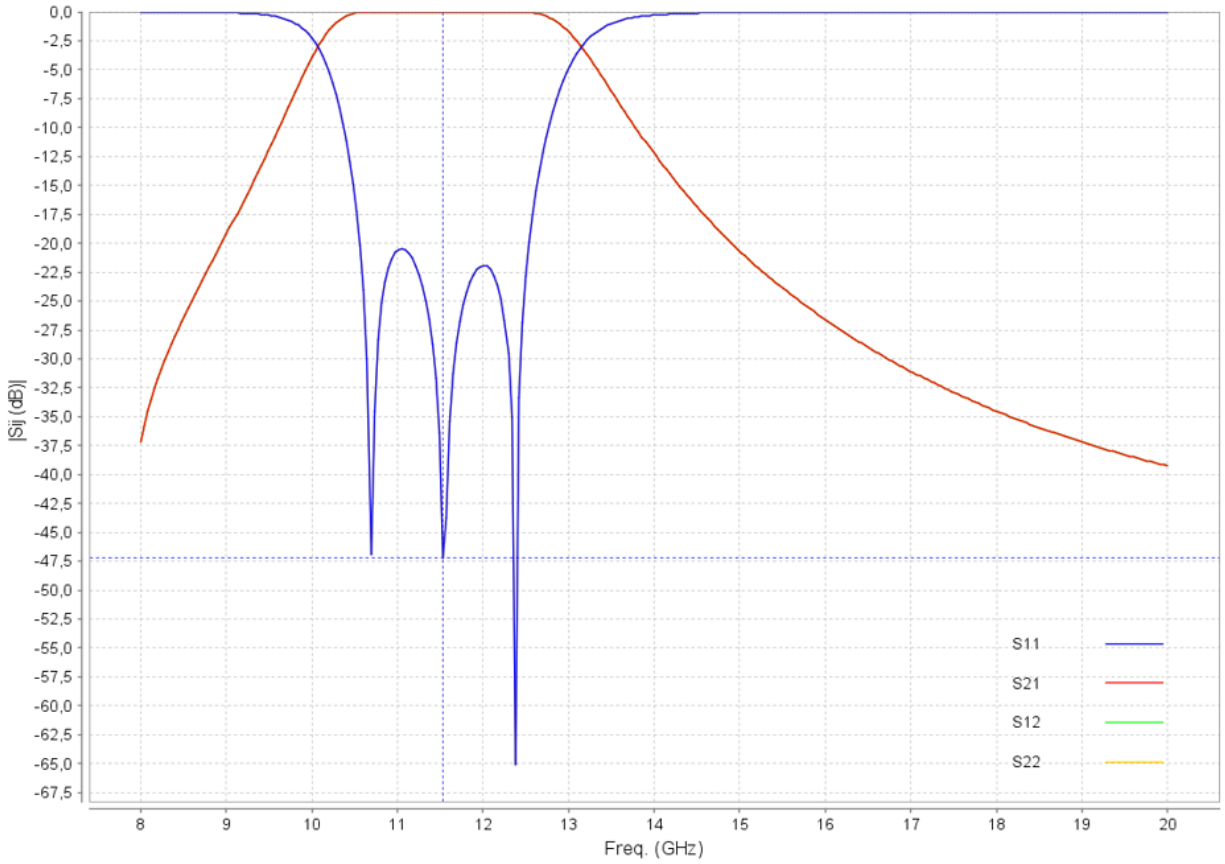

Figure 3.21: S parameters reponse of the optimized design for the 2 GHz bandwidth filter.

The final dimensions of the filter are shown in Table 3.13.

Variable	*Value* (mm)
$Port1a$	19.05
$Port1b$	9.525
$Port1l$	10
$ap_1 = ap_3$	14.1
$bp_1 = bp_3$	1.14
$l_{th_1} = l_{th3}$	0.1
l	5.45
ap_2	13.91
bp_2	0.22
l_{th2}	0.12

Table 3.13: Final dimensions for the 2 GHz bandwidth filter.

In Table 3.14 we show the comparative between the initial and the final dimensions of the filter.

Variable	*Initial value* (mm)	*Final value* (mm)	*Relative error*
$Port1a$	19.05	19.05	-
$Port1b$	9.525	9.525	-
$Port1l$	10	10	-
$ap_1 = ap_3$	13.5	14.1	0.04
$bp_1 = bp_3$	2.6	1.14	-1.28
$l_{th_1} = l_{th3}$	2	0.1	-0.95
l	3	5.45	0.45
ap_2	13.5	13.91	0.029
bp_2	2.6	0.22	-0.92
l_{th2}	2	0.12	-0.94

Table 3.14: Comparative between the initial and final dimensions for the 2 GHz bandwidth filter.

The optimized geometry for this design is shown in Fig. 3.22. The total physical dimensions for this filter are 19.05 mm $\times$ 9.525 mm $\times$ 31.22 mm, and dividing by $\lambda = \frac{c}{f_0} = 0.0261$, we obtain a filter of electrical dimensions 0.73 $\times$ 0.365 $\times$ 1.197.

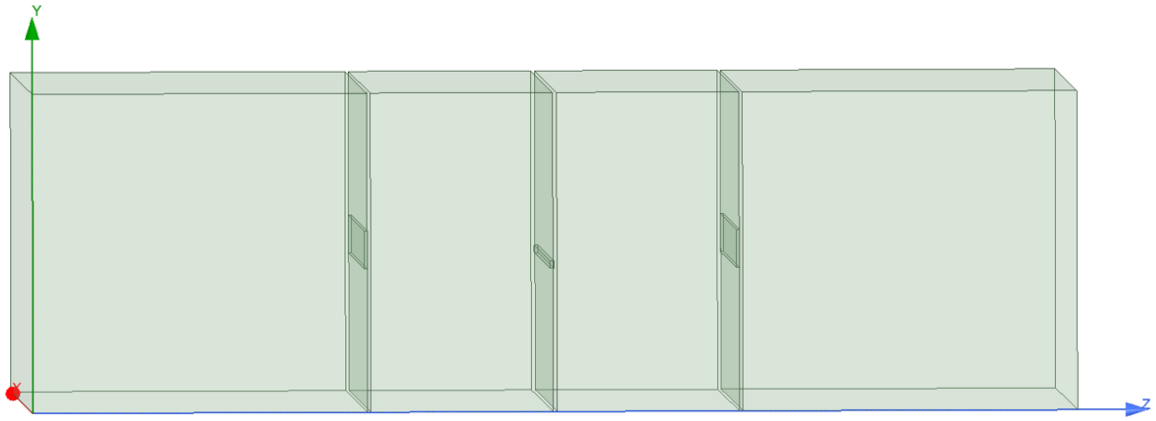

Figure 3.22: Optimized geometry for the 2 GHz bandwidth filter.

$$\begin{cases} \text{Physical dimensions:} \\ 19.05 \text{ mm} \times 9.525 \text{ mm} \times 31.22 \text{ mm} \end{cases} \longrightarrow \begin{cases} \text{Electrical dimensions:} \\ 0.73 \times 0.365 \times 1.197 \end{cases}$$

Now we are going to introduce two transmission zeros to the design. For this, we add a step discontinuity between the source and the first resonator, and another one between the last resonator and the load. In this case the dimensions of the step discontinuities are 25.05 mm $\times$ 15.525 mm $\times$ 2. The design is shown in Fig. 3.23.

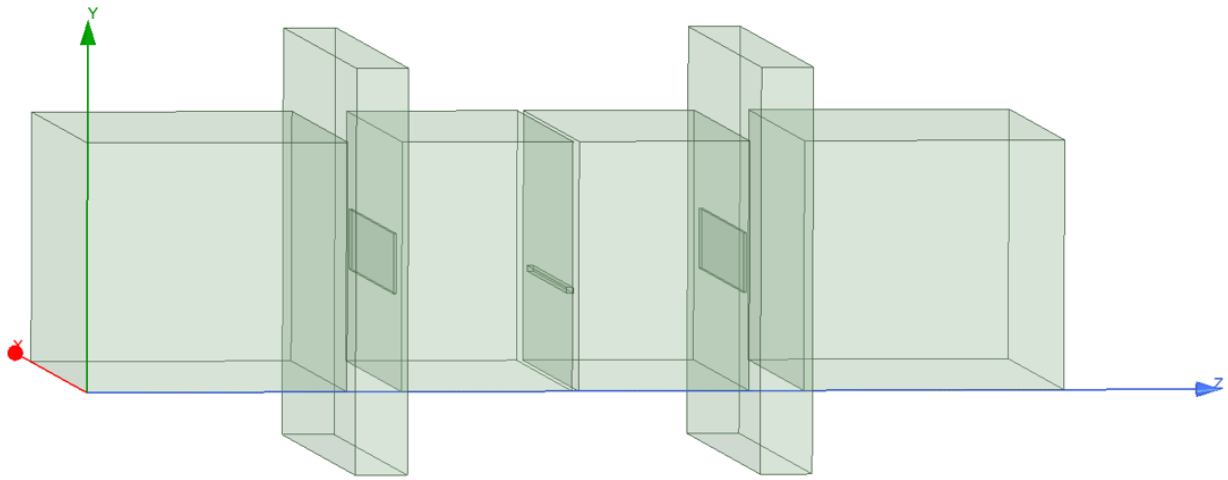

Figure 3.23: Optimized geometry for the 2 GHz bandwidth filter with two step discontinuities.

In Fig. 3.24 we can observe the frequency response and in Table 3.15 we can see the final dimensions of the filter with this step discontinuity.

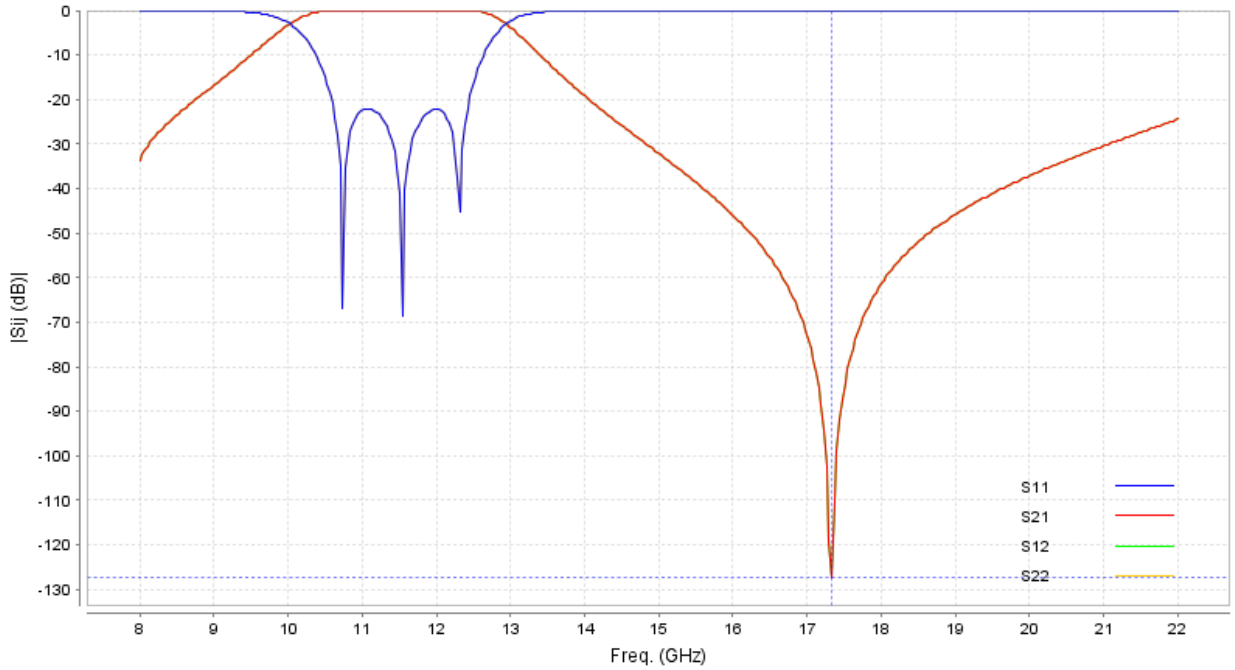

Figure 3.24: S parameters response of the 2 GHz bandwidth filter when adding a 25.05 mm × 15.525 mm × 2 mm step discontinuity.

Variable	*Value* (mm)
$Port1a$	19.05
$Port1b$	9.525
$Port1l$	10
$ap_1 = ap_3$	15.22
$bp_1 = bp_3$	2.29
$l_{th_1} = l_{th3}$	0.1
l	6.56
a_2	13.68
b_2	0.22
l_{th2}	0.24
a_{disc}	25.05
b_{disc}	15.525
l_{disc}	2

Table 3.15: Final dimensions for the 1 GHz bandwidth filter when adding a 25.05 mm × 15.525 mm × 2 mm step discontinuity.

The total physical dimensions of this filter are 25.05 mm × 15.525 mm × 37.56 mm. If we divide these physical dimensions by $\lambda = \frac{c}{f_0} = 0.0261$, we obtain a filter of electrical dimensions 0.73 × 0.365 × 1.44.

$$\begin{cases} \text{Physical dimensions:} \\ 25.05 \text{ mm} \times 15.525 \text{ mm} \times 37.56 \text{ mm} \end{cases} \longrightarrow \begin{cases} \text{Electrical dimensions:} \\ 0.73 \times 0.365 \times 1.44 \end{cases}$$

Finally, to show that the two transmission zeros can be controlled independently, we change the length of the output step discontinuity to 1.8 mm. Therefore, as we have studied in Chapter 2, the frequency of this transmission zero gets a little bit higher. It should be noted as well that the optimized filters are very sensitive, so all these modifications must be done slowly while readjusting the filter. The frequency response of this asymmetric filter with two differenciated transmission zeros is shown in Fig. 3.25.

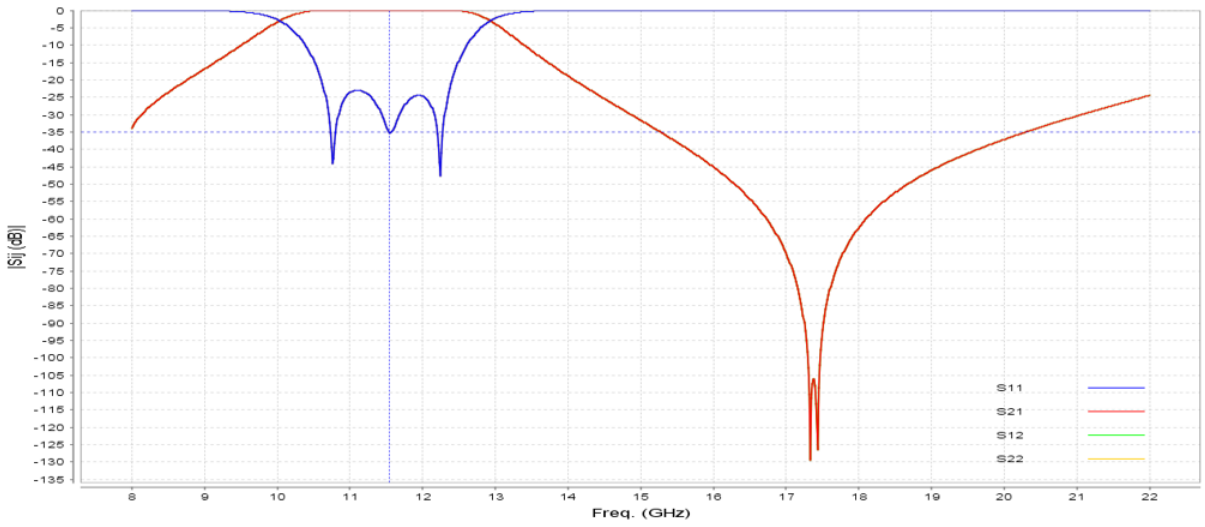

Figure 3.25: S parameters response of the 2 Ghz bandwidth filter when adding two differenciated transmission zeros.

3.5. Advantages of the proposed technology

In this section we are going to outline the advantages of the technology proposed in this bachelor thesis, based on resonant apertures, with respect to the technology based on resonant cavities. For this, we are going to compare two filters with a center frequency (f_0) of 11.5 GHz, a 500 MHz bandwidth and a return loss level of 22 dB. Therefore, these two filters have the same initial requirements but are based on two different technologies. This will allow us to compare them in terms of size and spurious free range (SFR). The spurious free range (SFR) is defined in [7] as:

$$SFR\ (\%) = \frac{|f_{unwanted\ mode} - f_{selected\ mode}|}{f_{selected\ mode}}, \tag{3.4}$$

where $f_{unwanted\ mode}$ is the resonant frequency of the nearest unwanted mode, and $f_{selected\ mode}$ is the resonant frequency of the mode we are working with.
In Fig. 3.26 we can see the out of band frequency response of the filter using resonant apertures.

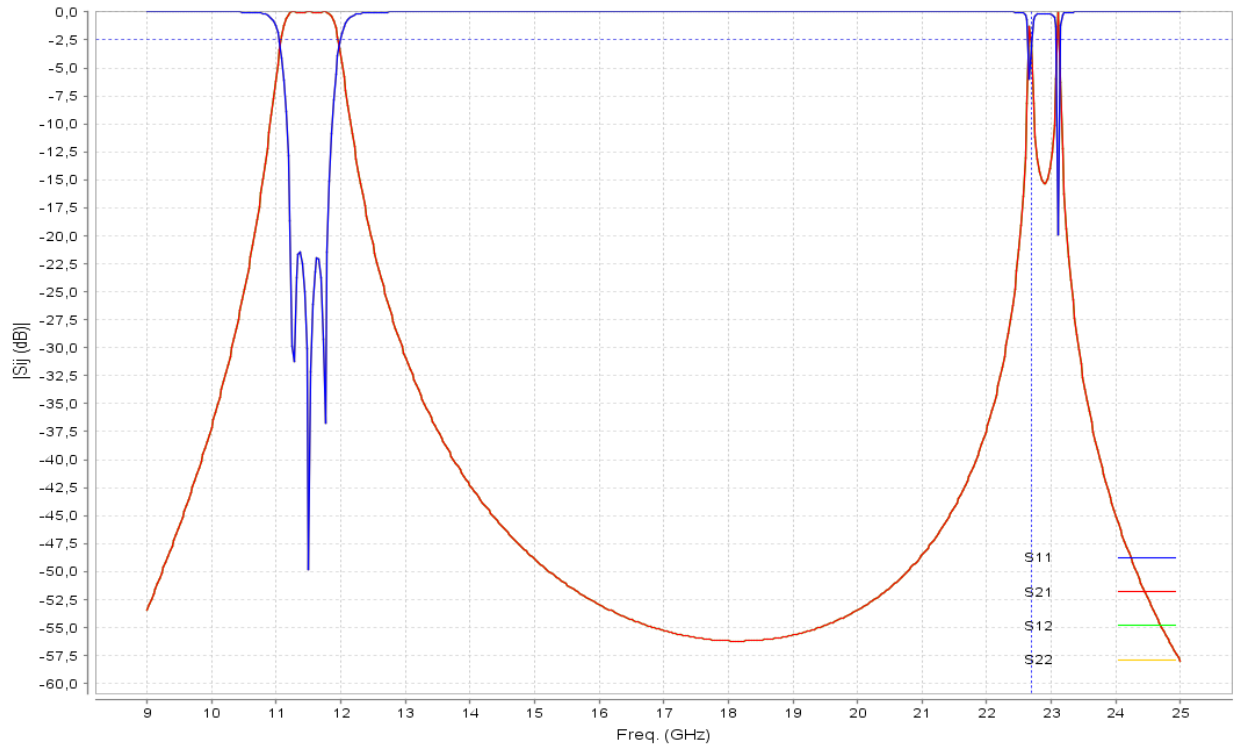

Figure 3.26: Out of band response of the 500 MHz filter using resonant apertures.

In Fig. 3.27 we can see the out of band frequency response of the filter using resonant cavities.

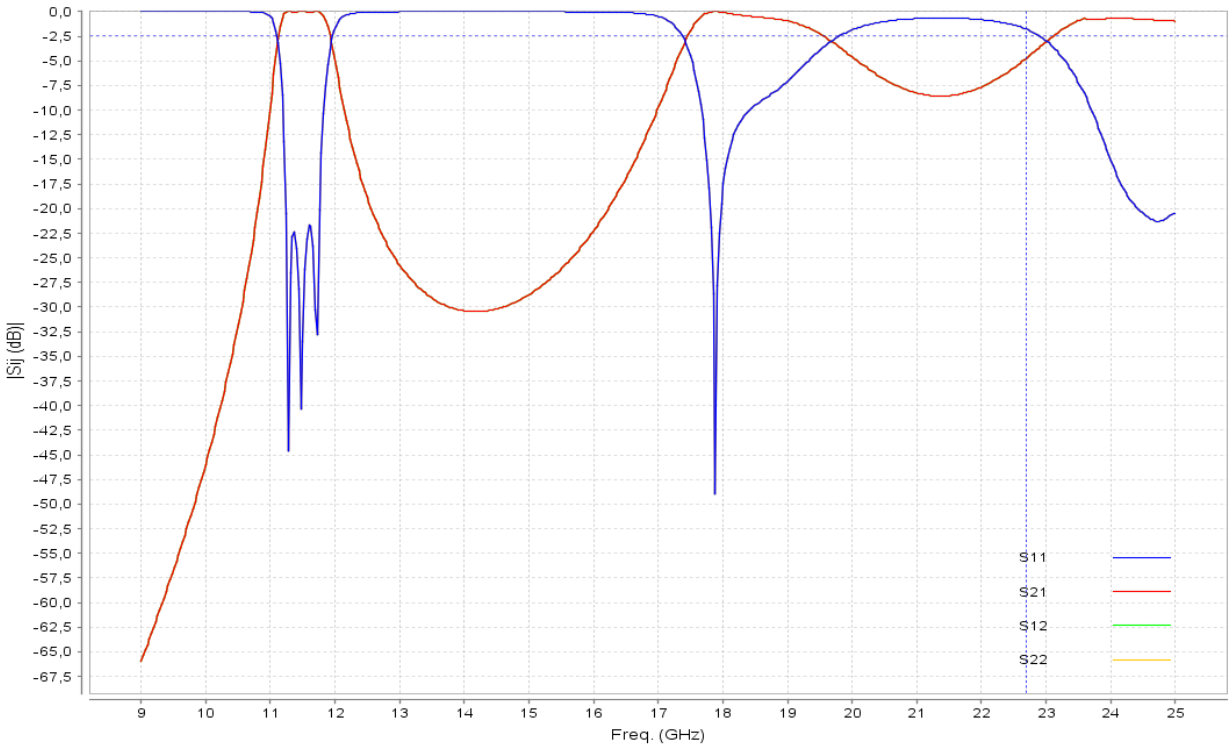

Figure 3.27: Out of band response of the 500 MHz filter using resonant cavities.

We can see in Fig. 3.26 that in this case the spurious free band extends up to 22.8 GHz, whereas in Fig. 3.27 we see that the spurious free band when using resonant cavities extends up to 18 GHz. In Fig. 3.28 we can see the comparison between the geometries for the two filters.

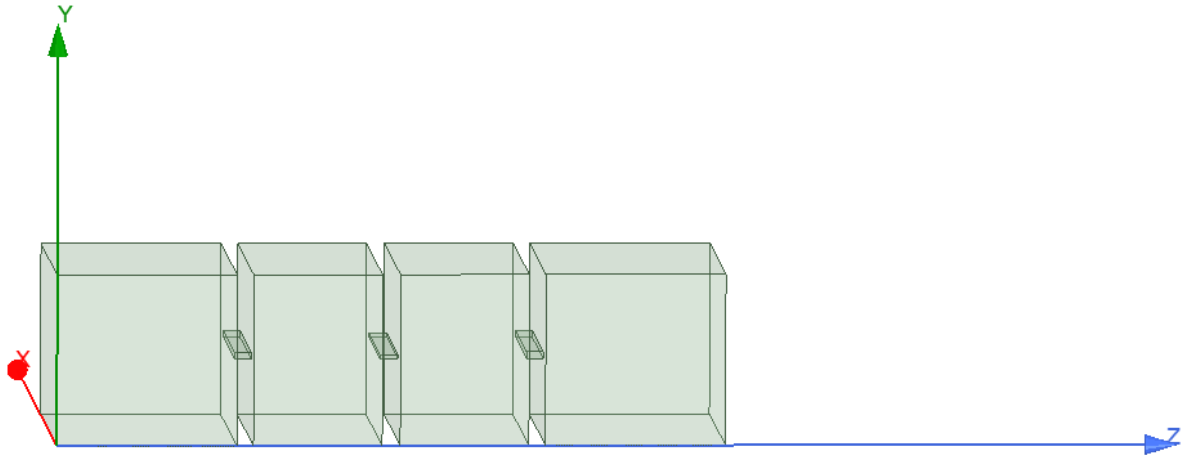

(a) Optimized geometry of the filter based in resonant apertures.

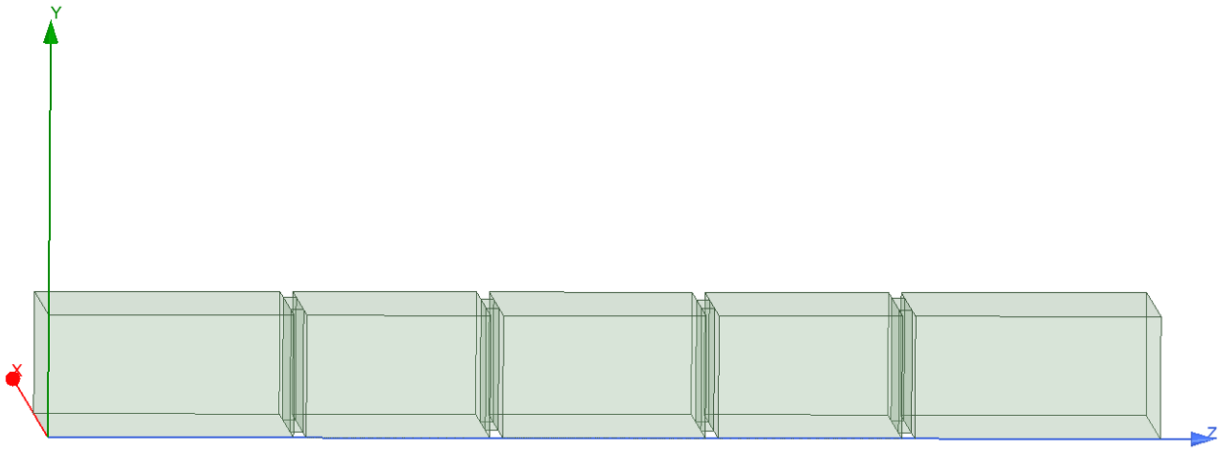

Figure 3.28: Optimized geometry of the filter based in resonant cavities.

The comparison between the two filters in terms of size and spurious free range (SFR) is shown in Table 3.16.

Technology	*Size* (mm)	*SFR* (%)
Resonant apertures	37.14	97.3
Resonant cavities	86.33	55.47

Table 3.16: Comparative between the two filters under study.

We can observe that the technology proposed in this project, based in resonant apertures, leads to a smaller filter size, due to the fact that the resonance is produced by the discontinuities between the guide sections and the apertures, and therefore we reduce the total length of the filter when comparing with filters based in $\lambda/2$ resonators. Besides, we show that this new technology presents a wider spurious free range. However, filters based in resonant cavities have usually Q_u factors around 5000, while in the proposed technology, the range of values for the unloaded quality factor (Q_u) goes from 300 to 3000. Therefore, if we wanted to compare these two technologies in terms of Q_u, we should design a filter based in resonant apertures with big sizes of apertures.

Chapter 4

Conclusions and further work

4.1. Conclusions

In this project a new technology based on resonant apertures for the implementation of waveguide filters has been presented. In Chapter 2 we have shown how to obtain the needed parameters for the characterization of the technology and how to implement transmission zeros with the proposed technology. In Chapter 3 we have explained how to design filters from the initial requirements using the figures and tables obtained in Chapter 2. After obtaining the initial point of the filter, we have performed both a manual optimization step and a second optimization using a comercial optimizator (FEST3D). Besides, we have also implemented transmission zeros in some of the designs shown in Chapter 3. Finally, we have outlined the advantages of this new technology in terms of size and spurious free range, comparing it with a standard technology based on resonant cavities.

4.2. Further work

The work presented in this bachelor thesis opens, among others, the following future works:

- Manufacture of the presented filters in order to compare the simulated response with the experimental one.
- During the calculation of the Q_u factor, we observed a drift in the resonant frequency f_0 when changing the length of the input/output ports. A future work could be to include an aditional element to the design in forder to have more control of the coupling.
- In this work it has been studied that the bigger the resonators are, the higher the Q_u factor will be. Therefore, a future work can be to carry out design strategies that lead to higher Q_u factors.
- This new technology opens the oportunity of designing new filters with different specifications from the ones in this project and for different applications. In particular, more complex filters with higher orders and complex coupling topologies could be envisaged.

Bibliography

[1] *https://ourworld.unu.edu/en/how-things-work-environmental-satellites*

[2] *https://www.nasa.gov/audience/forstudents/5-8/features/nasa-knows/what-is-a-satellite-58.html*

[3] Cameron, R. J., Mansour, R., and Kudsia, C. M. (2007). *Microwave Filters for Communication Systems: Fundamentals, Design and Applications.* John Wiley & Sons, Inc.

[4] Marcuvitz, N. (1986). *Waveguide Handbook.* Institution of Electrical Engineers, GBR.

[5] Vallerotonda, P., Pellicia, L., Tomassoni, C., Cacciamani, F., Sorrentino, R., Galdeano, J., and Ernst, C. (2019). *Compact Waveguide Bandpass Filters for Broadband Space Applications in C and Ku-Bands.* European Microwavw Conference in Central Europe (EuMCE), Prague, Czech Republic, 2019, pp. 116-119.

[6] *https://www.ansys.com/products/electronics/ansys-hfss*

[7] Lorente, J. A. (2013). *Techniques for Loss Reduction in Waveguide Filters. Phd thesis,* UPCT, Cartagena, Spain.

[8] Pozar, D. M. (2012). *Microwave Engineering* John Wiley & Sons, Inc.

[9] *https://www.3ds.com/products-services/simulia/products/fest3d*

[10] *https://es.mathworks.com/products/matlab.html*